An analytical approach for modelling the vibroacoustic behaviour of a heavy fluid-loaded plate near a free surface

Jamie Kha, Mahmoud Karimi, Laurent Maxit, Alex Skvortsov, Ray Kirby

An analytical approach for modelling the vibroacoustic behavior of a heavy fluid-loaded plate near a free surface

Jamie Kha[a], Mahmoud Karimi[a], Laurent Maxit[b], Alex Skvortsov[c], Ray Kirby[a]

[a] *Centre for Audio, Acoustics and Vibration, University of Technology Sydney, Sydney, Australia*
[b] *Univ Lyon, INSA–Lyon, Laboratoire Vibrations-Acoustique (LVA), 25 bis, av. Jean Capelle, F-69621, Villeurbanne Cedex, France*
[c] *Maritime Division, Defence Science and Technology, Melbourne, Australia*

Abstract

Predictions of the vibroacoustic response of a point-force excited baffled thin rectangular plate immersed in a heavy fluid and near a free surface are presented using an analytical model. The equations of motion are solved by Fourier analysis, where the eigenfunctions of plate vibration form the basis of spatial expansion for fluid loading. Vibroacoustic indicators, including the plate velocity, acoustic pressure, and acoustic power, are predicted using the analytical approach and verification is performed by comparison with finite element simulations. The results have shown that variations in the height of the free surface can have a significant effect on these indicators. From the vibration response, added mass effect due to heavy fluid loading is altered and further investigated with the explicit evaluation of an added mass ratio for different free surface heights for the first five plate modes. For a given height of a free surface, standing waves can form between the free surface and baffled plate at specific excitation frequencies and slightly alters the acoustic pressure spectra. This condition also presents an effect on the acoustic power, where the first standing wave frequency dictates the efficient sound radiation to the far field.

Keywords: vibroacoustic response, free surface, heavy fluid loading, baffled flat plate, analytical model

1. Introduction

Vibroacoustic responses of elastic structures surrounded by a heavy fluid, typically water, has been a major focus of the analysis of fluid-structure interactions, as studied in [1] and Refs therein. It is known that the surrounding fluid can significantly affect the response of a structure [2, 3], and thus understanding the response of excited structures with various modelling techniques and experimentation is important. The vibroacoustic behavior of a structure can be understood by the prediction of vibroacoustic indicators such as its surface velocity and sound radiation. These indicators are of practical importance in underwater

engineering as it presents the structural and acoustic response of a system in relation to its hydrodynamic performance. The accurate prediction of the fluid-structure response is then necessary to better achieve optimizations in its vibroacoustical behavior. These optimizations include noise mitigation strategies such as passive control [4, 5, 6, 7] or active control [8, 9, 10]. Predictions of vibroacoustic indicators can be accomplished by analytical modelling which presents an advantage over numerical methods, such as finite element and boundary element methods, and experimentation, with its inherent computational efficiency and ease of numerical implementations of parametric studies. Especially in fluid-structure scenarios in which the fluid domain is heavy, finite and significantly larger than the structure of interest, it can be difficult or infeasible to properly capture the acoustics using numerical simulations or experimentation. In literature, the analytical modelling of elastic plates is a focus of fluid-structure interactions due to its simplicity and application as a first-order approximation, as the plate model can provide a heuristic insight into the vibroacoustic behavior to more complicated geometries such as a cylindrical shell - which has relevant maritime applications.

Free vibration analysis of plates coupled with heavy fluid and near a free surface has been widely studied to understand how fluid layer thickness can affect its structural response. When concerned only about vibration, the governing equation for the fluid domain is the Laplace equation, which ignores the compressibility of the fluid and time-dependency of acoustic waves that propagate into the acoustic medium. Studies concerning the free vibration of circular plates were first considered. Amabili [11] investigated the free vibrations of circular and annular plates, embedded in a rigid wall with different boundary conditions, and with a fluid layer limited by a free surface or rigid wall. The assumed mode method was employed, where the wet mode shapes of the plates was assumed to be equivalent to the dry mode shapes. It was shown that natural frequencies of the plate decease with fluid depth and the assumed mode method was sufficiently accurate compared to the Rayleigh-Ritz method. A similar work was performed by Kwak and Han [12], where free-edge annular plates completely immersed in fluid was considered. The free vibration of circular plates was also found in studies of fluid-filled cylindrical containers, where a method of partial domains was applied. Askari and Daneshmand [13] performed free vibration analysis on the elastic bottom plate of a partially-filled fluid container with an internal body by dividing and solving the partial fluid domains. The Rayleigh-Ritz method was then employed to develop a parametric study on the effect of the fluid level, nodal diameter number, and nodal circle number on the natural frequencies and modes of the plate. A similar study was performed for free or fully clamped circular plates submerged in a fluid-filled cylindrical container with results compared against experimentation [14]. For rectangular plates, Ergin and Uğurlu [15] performed a natural frequency analysis on vertically cantilevered plates that were partially submerged in a finite fluid.

The analysis utilized an image-source method to account for the free surface effect from the plate submergence. These results were compared against those generated by Kerboua et al. [16], in an extensive study of rectangular plates floating on a free surface, vertically cantilevered in a fluid-filled container, and completely submerged. This study utilized a hybrid method of finite element and analytical modelling based on Sander's shell theory to develop a more efficient approach. Hosseini-Hashimi et al. [17] then investigated the effect of finite fluid depth levels on free vibration of Mindlin plates, which was extended by Cho et al. [18] in a study of stiffened plates. Extensive work was also found in more complex fluid-plate scenarios such as considering the effect of a crack on a submerged plate [19, 20, 21], and plates of different material compositions [22, 23, 24].

Aside from the free vibration, plates under excitation are of relevant interest, where forced vibration studies consider an excitation in the analysis of the structural response. For the fluid-loaded plate with a free surface, Soedel and Soedel [25] provided an analytical framework for the analysis of free and forced vibration of a plate supporting a freely sloshing surface liquid, where the harmonic point force excitation is presented as an orthogonal plate-liquid modes. Meylan [26] presented a general analytical approach to solve the forced vibration of an arbitrary thin plate floating on the free surface of an infinite fluid by applying the appropriate Green's function to the fluid domain and solving a variational equation with the Rayleigh-Ritz method. Hosseini-Hashimi et al. [27, 28] studied the behavior of Mindlin plates on Pasternak foundations submerged from a finite depth of fluid and under linearly varying in-plane loads, with an extensive parametric study that involves the effect of the loading factors and fluid level. Cho et al. [29] extends this work by presenting Mindlin plates and stiffened plates under harmonic point excitation with surface velocity spectra compared against coupled finite element and boundary element results. Apart from the plate-fluid-free surface system, there has been considerable research into the plate-fluid-rigid wall system. Akbarov et al. provides the frequency response of the stress and velocity of a system composed of a highly elastic plate, compressible viscous fluid and rigid wall system, with investigation into the effect of imposing initial strains on the plate [30], and a plate moving velocity [31]. Akbarov and Huseynova continues this work for an orthotropic plate, compressible viscous fluid and rigid wall system [32] and with the effect of moving point load [33]. Further extension can be found by a recent work of Koçal [34], where the dynamical behavior of the moving plate under time-harmonic forces was investigated with various rheological parameters.

It is necessary to capture the acoustics of the submerged plate near a free surface to develop a complete understanding of the fluid-structure system. Acoustics of a fluid-loaded plate near a free surface can be studied with the Helmholtz equation, which is necessary to solve for the acoustic wave propagation in the

fluid that is coupled with the structure. Earlier works investigate the acoustics of a plate under heavy fluid loading and immersed in a semiinfinite fluid domain (no free surface). To solve the fluid-plate problem, a direct approach can be utilized by implementing the in-vacuo eigenfunctions of the plate as the basis of the Fourier decomposition of the fluid loading as demonstrated by Sandman [35] in a study of fluid-loaded baffled simply supported plates with attached concentrated mass loadings in a semiinfinite fluid domain. This analytical approach was used in Gu and Fuller's [8] investigation of active noise control of a fluid-loaded plate. Berry [36] proposed an alternate approach to solve the sound radiation of fluid-loaded plates with various elastic boundary conditions using variational formulation solved with the Rayleigh-Ritz method. This analytical approach was extended by Nelisse et al. [37], who provided a generalized approach for acoustic radiation of both unbaffled and baffled plates. Arenas and Crocker [38] focused on the acoustic radiation resistance matrix, presenting an efficient method to evaluate the sound radiation from planar structures by using the volume velocity vector of the discretised vibrating surface. Aside from a plate in a semiinfinite fluid domain, literature specific to the vibroacoustic response of a plate with a fluid layer is limited. Experimental investigation has been performed by Génevaux [39] in a study of the vibroacoustic behavior of a plate with a fluid layer in a gas volume at the lower frequency range. Sound radiation was investigated by Sun et al. [40] with a plate-fluid-rigid wall system where the effect of a fluid layer of a force-driven baffled plate was studied. Though the effect of a free surface is not considered, it was demonstrated that the presence of a fluid layer has significant effect on the efficiency of acoustic radiation modes of the plate. Relevant to the free surface effect is the cylindrical shell in a waveguide domain, which is typically composed of a seabed and free surface. These investigations simulate shallow water effects where the height of the free surface to the seabed is significantly low. Investigations into the effect of a waveguide or layer of fluid are commonly solved with the image-source method [41]. The method has been applied to an early work of an infinite cylindrical shell with a free surface only [42] and provided a precursor formulation for the shallow water boundary value problem for cylindrical shells [43, 44, 45]. However, to the best knowledge of the authors, there are no studies on the acoustic radiation from submerged plates near a free surface. The present work, for the first time, develops an analytical model that captures both vibration and acoustic (vibroacoustic) behavior of a heavy fluid loaded plate near a free surface.

This work herein presents findings from the effect of a free surface on the vibroacoustic response of a heavy fluid-loaded thin rectangular baffled plate due to a point force excitation using an analytical approach. To achieve this, the thin plate response is modelled using modal decomposition of an in-vacuo plate, and the acoustic waves from the transverse motion of the plate are solved for with the Helmholtz equation.

The modal amplitudes of the transversal displacement of the plate can then be solved from its radiation impedance equation, which has the characteristics of the fluid domain embedded into it via a Rayleigh-like integral where the integrand includes the Green's function solution to the Helmholtz equation. The vibroacoustic behavior of a flat plate near a free surface is investigated by evaluating the plate velocity, acoustic pressure and radiated sound power. Predictions of these vibroacoustic indicators for a plate near a free surface are compared against corresponding results generated from a baffled plate in semiinfinite domain, and verification is achieved by comparing results against 3D finite element simulations using COMSOL. Numerical investigation into the free surface effect on the structural and acoustic response of the plate is further explored in relation to the added mass effect, standing waves criterion, far field pressure and wavenumber contribution to the total acoustic power. The radiated pressure in the fluid layer and sound power are predicted and analyzed as a function of the depth of plate submergence from the free surface.

2. Model

2.1. Fluid-loaded plate near a free surface

As shown in Fig. 1, consider an elastic rectangular baffled plate with a free surface at a height H above the plate, with a, b, h being respectively the length, width and thickness of the plate. The plate is simply supported on its four edges and is made of an elastic material of Young's modulus E, Poisson's ratio ν, density ρ_p, and structural damping loss factor η. It is immersed in a fluid with density ρ_0 and sound speed c_0. The infinite baffle is a rigid boundary condition, while, the fluid domain is a waveguide that is formed by the infinite baffle and free surface. The free surface is considered as a pressure release condition. The cartesian coordinate system $\mathbf{x} = (x, y, z)$ is positioned at a corner of the plate with the baffled plate in the x-y plane. Force excitation and fluid loading are exhibited in the z direction.

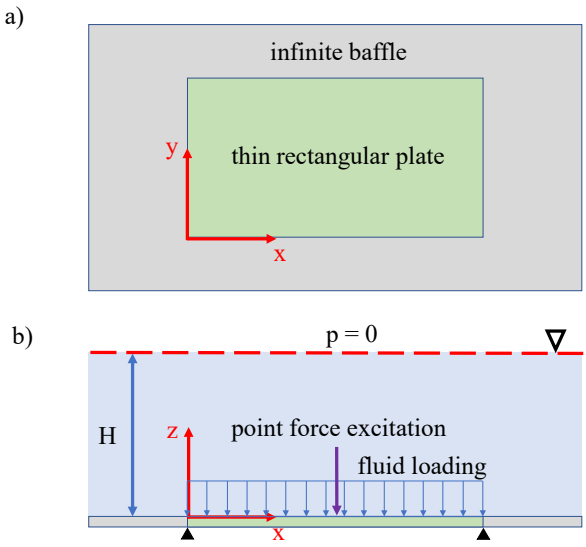

Figure 1: a) Top view and b) side view of a fluid-loaded baffled plate with a free surface at $z = H$.

The classical thin plate theory is used here which ignores transverse shear deformation. This deformation is generally negligible for thin plates (i.e., the ratio of the plate thickness to the smallest in-plane dimension does not exceed 0.02 [46]) and for low excitation frequencies (i.e. frequencies below 0.7 times the coincidence frequency [47]). The governing equation for the transverse motion of a plate in the frequency domain, with an assumed harmonic time (t) dependence of $e^{\mathrm{j}\omega t}$, is given by

$$D^{\star}\nabla^4 w\left(\mathbf{x_0},\omega\right) - \rho_p h\omega^2 w\left(\mathbf{x_0},\omega\right) = F\left(\mathbf{x_0}\right) + p_0\left(\mathbf{x_0},\omega\right) \tag{1}$$

where the nabla operator is defined as $\nabla^4 = \left[\dfrac{\partial^2}{\partial x^2} + \dfrac{\partial^2}{\partial y^2}\right]^2$, $D^{\star} = E^{\star}h^3/[12(1-\nu^2)]$ where $D^{\star}$ and $E^{\star}$ are the complex flexural rigidity of the plate and complex Young's modulus respectively, ω is the radial frequency, w is the plate transversal displacement, F is the applied external force, $p\left(\mathbf{x_0},\omega\right)$ is the fluid loading pressure and $\mathbf{x_0} = (x, y, 0)$ is a location on the surface of the plate. Structural damping is introduced in the model from a complex Young's modulus $E^{\star} = E\left(1 + \eta\mathrm{j}\right)$. The transversal displacement of the plate is expressed as a modal decomposition of the in-vacuo modes

$$w(\mathbf{x_0},\omega) = \sum_{m=1}^{\infty}\sum_{n=1}^{\infty} W_{mn}(\omega)\varphi_{mn}(\mathbf{x_0}), \tag{2}$$

where $\varphi_{mn}(\mathbf{x_0})$ are the plate mode shapes for a simply supported plate of mode (m, n) and is given by

$$\varphi_{mn}(\mathbf{x_0}) = \sqrt{\frac{2}{ab}}\sin\left(\frac{m\pi x}{a}\right)\sin\left(\frac{n\pi y}{b}\right). \tag{3}$$

The modal response of the plate can be obtained by introducing Eq. (2) into Eq. (1) and projecting the resulting expression by $\varphi_{rs}(\mathbf{x_0})$ where the orthogonal relation is

$$\int_0^b \int_0^a \varphi_{mn}(\mathbf{x_0}) \cdot \varphi_{rs}(\mathbf{x_0})\ dx\, dy = \delta_{rm}\delta_{sn} = \begin{cases} 1 & \text{if } r = m \text{ and } s = n, \\ 0 & \text{otherwise,} \end{cases} \tag{4}$$

with δ_{ij} as the Kroncker delta function defined by

$$\delta_{ij} = \begin{cases} 1 & \text{if } i = j, \\ 0 & \text{if } i \neq j, \end{cases} \tag{5}$$

$$\left[K^p_{rsmn} - \omega^2 M^p_{rsmn}\right] W_{mn} = f_{rs} + p_{rs}, \tag{6}$$

where

$$K^p_{rsmn} = D^\star \left[\left(\frac{m\pi}{a}\right)^2 + \left(\frac{n\pi}{b}\right)^2\right]^2 \delta_{rm}\delta_{sn} \tag{7}$$

is the stiffness of the plate,

$$M^p_{rsmn} = \rho_p h\, \delta_{rm}\delta_{sn} \tag{8}$$

is the mass of the plate,

$$f_{rs} = F_0\, \varphi_{rs}(\mathbf{x_f}), \tag{9}$$

is the modal coefficient of a point force excitation $F(\mathbf{x_f}) = F_0\, \delta\left(x - x_f\right)\left(y - y_f\right)$ where $\mathbf{x_f} = \left(x_f, y_f\right) \in \mathbf{x_0}$ with F_0 as the magnitude of the force, and

$$p_{rs} = \int_0^b \int_0^a p_0(\mathbf{x_0}) \cdot \varphi_{rs}(\mathbf{x_0})\ dx\, dy. \tag{10}$$

is the modal pressure.

To compute the modal coefficients of the transversal displacement of the plate W_{mn}, the pressure at $z = 0$ should be determined in order to evaluate the modal pressure, p_{rs}. Velocity potential is first considered and will be related to the acoustic pressure by the following relation

$$p(\mathbf{x}, \omega) = -\mathrm{j}\omega\rho_0 \Psi(\mathbf{x}, \omega). \tag{11}$$

In the fluid domain, the velocity potential should satisfy the Helmholtz equation

$$\nabla^2\Psi + k_0^2\Psi = 0, \tag{12}$$

where $k_0 = \omega/c_0$ is the acoustic wavenumber. Whereas at the boundaries, the conditions are: for $z = 0$

$$\left(\frac{\partial \Psi}{\partial z}\right)_{z=0} = V(\mathbf{x_0}, \omega) = \begin{cases} v(\mathbf{x_0}, \omega) = \mathrm{j}\omega \sum_{m=1}^{\infty} \sum_{n=1}^{\infty} W_{mn}(\omega) \varphi_{mn}(\mathbf{x_0}) & \{0 \le x \le a, 0 \le y \le b\}, \\ 0 & \text{(off the plate)}, \end{cases} \tag{13}$$

where $v(\mathbf{x_0}, \omega)$ is the plate velocity, and for $z = H$, the pressure release condition $\Psi(x, y, H, \omega) = 0$ is considered. Applying the Fourier transform in the x and y directions to the Helmholtz equation the expression becomes an ordinary differential equation

$$\frac{\partial^2 \Psi^*}{\partial z^2} = \gamma^2 \Psi^* \quad \text{with} \quad \gamma^2 = k_x^2 + k_y^2 - k_0^2, \tag{14}$$

where the Fourier transform and inverse Fourier trasnform are defined respectively as

$$\Psi^*\left(k_x, k_y, z\right) = \int_{-\infty}^{\infty} \int_{-\infty}^{\infty} \Psi(x, y, z) e^{-\mathrm{j}(k_x x + k_y y)} \, dxdy, \tag{15}$$

$$\Psi(x, y, z) = \frac{1}{4\pi^2} \int_{-\infty}^{\infty} \int_{-\infty}^{\infty} \Psi^*\left(k_x, k_y, z\right) e^{\mathrm{j}(k_x x + k_y y)} \, dk_x dk_y. \tag{16}$$

The boundary condition from Eq. (13) becomes

$$\frac{\partial \Psi^*}{\partial z} = V^*\left(k_x, k_y\right), \tag{17}$$

Using the boundary conditions on the plate with the pressure release condition of a free surface, the Helmholtz equation can be solved and the spectral velocity potential is found to be

$$\Psi^*\left(k_x, k_y, z\right) = V^*\left(k_x, k_y\right) G^*\left(k_x, k_y, z\right), \tag{18}$$

with

$$G^*\left(k_x, k_y, z\right) = \frac{e^{\gamma(z-H)} - e^{-\gamma(z-H)}}{\gamma\left(e^{\gamma H} + e^{-\gamma H}\right)}. \tag{19}$$

If $k_x^2 + k_y^2 < k_0^2$, i.e. for wavenumbers inside the acoustic radiation circle (defined by $k_x^2 + k_y^2 = k_0^2$), γ is purely imaginary if no damping is considered in the fluid, and k_z is defined by $k_z = \sqrt{k_0^2 - k_x^2 - k_y^2}$. Then, $\gamma = \pm \mathrm{j} k_z$ and G^* can be expressed as $G^*\left(k_x, k_y, z\right) = \dfrac{\sin\left[k_z(z-H)\right]}{k_z \cos\left(k_z H\right)}$. The condition of $\cos\left(k_z H\right) \neq 0$ results in standing waves at $k_z = \pi(2N+1)/(2H)$ where $N = 0, 1, 2, 3...$ or resonant frequencies $f = c_0(2N+1)/(4H)$, which depend on the free surface height. If $k_x^2 + k_y^2 > k_0^2$, i.e. for wavenumbers outside the acoustic radiation circle, γ is purely real and $k_z = \sqrt{k_x^2 + k_y^2 - k_0^2}$, and $G^*\left(k_x, k_y, z\right) = \dfrac{\sinh\left[k_z(z-H)\right]}{k_z \cosh\left(k_z H\right)}$. Practically, the acoustic wavenumber is complex i.e. $k_0' = k_0\left(1 - \eta_f \mathrm{j}\right)$, where $\eta_f << 1$ is fluid damping, and $k_z' = \kappa_1 \pm \kappa_2 \mathrm{j}$, where κ_1, κ_2 are approximated in Appendix A.

The spectral velocity potential can be expressed as a product of two functions $\Psi^*\left(k_x, k_y, z\right) = V^*\left(k_x, k_y\right) \cdot G^*\left(k_x, k_y, z\right)$. To determine the velocity potential in the spatial domain, the inverse Fourier transform of the spectral velocity potential is performed. In this particular case, the inverse Fourier transform is the convolution of the inverse Fourier transform of each of the product terms. Considering the plate boundary conditions from Eq. (13), the velocity potential in the spatial domain is then expressed as

$$\Psi\left(\mathbf{x}\right) = \int_0^b \int_0^a v\left(x_1, y_1\right) G\left(x - x_1, y - y_1, z\right) dx_1 dy_1, \tag{20}$$

where $G\left(x - x_1, y - y_1, z\right)$ is the spatially shifted inverse Fourier transform of $G^*\left(k_x, k_y, z\right)$. To obtain the function G, first consider that the trigonometric functions can be expressed in terms of exponential functions

$$G^*\left(k_x, k_y, z\right) = -\left[\frac{e^{-\gamma z}}{\gamma} - \frac{e^{\gamma z}}{\gamma}\frac{e^{-2H\gamma}}{1 + e^{-2H\gamma}} - \frac{e^{-\gamma z}}{\gamma}\frac{e^{-2H\gamma}}{1 + e^{-2H\gamma}}\right]. \tag{21}$$

In this form, it is identified that $\dfrac{e^{-2H\gamma}}{1 + e^{-2H\gamma}}$ is the limiting sum for a geometric series with a common ratio of $-e^{-2H\gamma}$, where $\left|e^{-2H\gamma}\right| < 1$

$$\frac{e^{-2H\gamma}}{1 + e^{-2H\gamma}} = \sum_{l=1}^{\infty} (-1)^{l+1} e^{-2Hl\gamma}. \tag{22}$$

For wavenumbers inside the acoustic radiation circle, $k_z' = \kappa_1 - \kappa_2 \mathrm{j}$ and the modulus of the common ratio is evaluated to be $\left|e^{-2Hjk_z'}\right| = e^{-2H\kappa_2}$ which is strictly less than 1. For wavenumbers outside the acoustic radiation circle, $k_z' = \kappa_1 + \kappa_2 \mathrm{j}$ and the modulus of the common ratio is $\left|e^{-2Hkz'}\right| = e^{-2H\kappa_1}$ which is also strictly less than 1. Therefore, applying Eq. (22) to Eq. (21), the Fourier transform of G can be expressed as a summation of exponential functions

$$G^*\left(k_x, k_y, z\right) = -\frac{1}{\gamma}e^{-\gamma z} + \frac{1}{\gamma}\sum_{l=1}^{\infty} (-1)^{l+1}\left[e^{-\gamma(2Hl - z)} + e^{-\gamma(2Hl + z)}\right]. \tag{23}$$

In this form, it becomes convenient to determine the function G by evaluating the spatially shifted inverse Fourier transform of $G^*\left(k_x, k_y, z\right)$ with the Weyl's integral applied commutatively [48, 49]

$$\frac{e^{-\mathrm{j}k_0'|r - r'|}}{|r - r'|} = -\frac{1}{2\pi}\int_{-\infty}^{\infty}\int_{-\infty}^{\infty} e^{\mathrm{j}\left[k_x(x - x') + k_y(y - y')\right]}\frac{e^{-\gamma|z - z'|}}{\gamma} dk_x dk_y, \tag{24}$$

The function $G\left(x - x_1, y - y_1, z\right)$ is determined to be

$$G\left(x - x_1, y - y_1, z\right) = \frac{1}{2\pi}\left\{\frac{e^{-\mathrm{j}k_0'R}}{R} - \sum_{l=0}^{\infty}(-1)^l\left[\frac{e^{-\mathrm{j}k_0'R_l^+}}{R_l^+} + \frac{e^{-\mathrm{j}k_0'R_l^-}}{R_l^-}\right]\right\}, \tag{25}$$

where $R = \sqrt{(x-x_1)^2 + (y-y_1)^2 + z^2}$ and $R_l^{\pm} = \sqrt{R^2 + (2H + 2lH \pm z)^2}$. At the surface of the plate $z = 0$, the function $G(x - x_1, y - y_1, 0)$ is simplified to be

$$G_{WG}(x-x_1, y-y_1) = G(x-x_1, y-y_1, 0) = \frac{1}{2\pi}\left\{\frac{e^{-\mathrm{j}k_0' R_0}}{R_0} - 2\sum_{l=0}^{\infty}(-1)^l \frac{e^{-\mathrm{j}k_0' R_l'}}{R_l'}\right\}, \tag{26}$$

where $R_0 = \sqrt{(x-x_1)^2 + (y-y_1)^2}$ is the distance between source points and a point of interest on the plate, and $R_l' = \sqrt{R_0^2 + (2H + 2lH)^2}$. The velocity potential, from substituting Eq. (13) to Eq. (20), is expressed as

$$\Psi(\mathbf{x_0}, \omega) = \mathrm{j}\omega \sum_{m=1}^{\infty}\sum_{n=1}^{\infty} W_{mn} \int_0^b \int_0^a \varphi_{mn}(\mathbf{x_1}) G_{WG}(x-x_1, y-y_1)\ \mathrm{d}x_1 \mathrm{d}y_1. \tag{27}$$

Using the relation from Eq. (11), the fluid loading pressure is presented as a Rayleigh-like integral

$$p_0(\mathbf{x_0}, \omega) = \rho_0 \omega^2 \sum_{m=1}^{\infty}\sum_{n=1}^{\infty} W_{mn} \int_0^b \int_0^a \varphi_{mn}(\mathbf{x_1}) \cdot G_{WG}(x-x_1, y-y_1)\ dx_1\, dy_1 \tag{28}$$

where G_{WG} is the familiar Green's function for the waveguide domain which can be alternatively derived from a method of images. Introducing Eq. (28) into Eq. (10), the modal pressure p_{rs} can be expressed as

$$p_{rs} = -\mathrm{j}\omega \sum_{m=1}^{\infty}\sum_{n=1}^{\infty} W_{mn} Z_{rsmn}^f, \tag{29}$$

with the fluid loading impedance expressed as

$$Z_{rsmn}^f = R_{rsmn}^f + \mathrm{j}\omega M_{rsmn}^f \tag{30}$$

$$= \mathrm{j}\omega\rho_0 \int_0^b \int_0^a \int_0^b \int_0^a \varphi_{mn}(\mathbf{x_1}) \varphi_{rs}(\mathbf{x_0}) G_{WG}(x-x_1, y-y_1)\ dx\, dy\, dx_1\, dy_1, \tag{31}$$

where R_{rsmn}^f is fluid resistance, and M_{rsmn}^f is the added mass due to fluid loading. By applying a change of variables to a non-dimensionalized cartesian coordinate system where $u = (x - x_1)/a$, $u_1 = x_1/a$, $v = (y - y_1)/b$, and $v_1 = y_1/b$.

$$Z_{rsmn}^f = \begin{cases} 4a^2b^2\mathrm{j}\omega\rho_0 \int_0^1 \int_0^1 \Phi_{rm}(u) \Phi_{sn}(v) \Omega(u,v)\, du dv & \text{for } r+m = \text{even} \wedge s+n = \text{even}, \\ 0 & \text{for } r+m = \text{odd} \vee s+n = \text{odd}. \end{cases} \tag{32}$$

The integrand consists of terms that are defined as:

$$\Omega(u,v) = \frac{1}{2\pi}\left\{\frac{e^{-\mathrm{j}k_0'\sqrt{a^2u^2 + b^2v^2}}}{\sqrt{a^2u^2 + b^2v^2}} - 2\sum_{l=0}^{\infty}(-1)^l \frac{e^{-\mathrm{j}k_0'\sqrt{a^2u^2 + b^2v^2 + (2H^2 + 2lH^2)}}}{\sqrt{a^2u^2 + b^2v^2 + (2H^2 + 2lH^2)}}\right\}, \tag{33}$$

and

$$\Phi_{\alpha\beta}(q) = \int_0^{1-q} \sin\left[\alpha\pi\left(q+q_1\right)\right] \sin\left(\beta\pi q_1\right) dq_1 = \tag{34}$$

$$\begin{cases} \dfrac{\sin\left[\pi\alpha\left(q-2\right)\right] + \sin\left(\pi\alpha q\right) - 2\pi\alpha\left(q-1\right)\cos\left(\pi\alpha q\right)}{4\pi\alpha} & \text{when } \alpha = \beta, \\ \dfrac{-\left(\beta+\alpha\right)\sin\left\{\pi\left[\beta\left(q-1\right)+r\right]\right\} + 2m\sin\left(\pi\alpha q\right) + \left(\alpha-\beta\right)\sin\left\{\pi\left[\beta\left(-q\right)+\beta+\alpha\right]\right\}}{2\pi\left(\beta-\alpha\right)\left(\beta+\alpha\right)} & \text{when } \alpha \neq \beta. \end{cases}$$

It should be noted that the fluid loading impedance Z has to be evaluated numerically. The integral in Eq. (32) becomes singular when $u = v = 0$ as $\Omega(u, v) \to \infty$. However, the singularity is integratable and it can be shown that an integration over an infinitely small surface surrounding this singularity tends to zero [50]. In this work, the Gaussian quadrature is applied to the numerical computation of the fluid loading impedance. Hence the singularity can be overcome by a judicious choice of the discretization points in the Gaussian procedure. Now, substituting Eq. (29) into Eq. (6) forms the following radiation impedance equation

$$\begin{bmatrix} I^{p+f}_{1111} & \dots & I^{p+f}_{111n} & I^{p+f}_{1121} & \dots & I^{p+f}_{11mn} \\ I^{p+f}_{1211} & & & & & \vdots \\ \vdots & & & & & \vdots \\ I^{p+f}_{rs11} & \dots & & \dots & & I^{p+f}_{rsmn} \end{bmatrix} \begin{bmatrix} W_{11} \\ W_{12} \\ \vdots \\ W_{mn} \end{bmatrix} = \begin{bmatrix} f_{11} \\ f_{12} \\ \vdots \\ f_{rs} \end{bmatrix}, \tag{35}$$

$$I^{p+f}_{rsmn} = K^{p}_{rsmn} + \mathrm{j}\omega R^{f}_{rsmn} - \omega^2 M^{f+p}_{rsmn} = K^{p}_{rsmn} + \mathrm{j}\omega Z^{f}_{rsmn} - \omega^2 M^{p}_{rsmn}, \tag{36}$$

where I^{p+f}_{rsmn} is the total impedance matrix and $M^{f+p}_{rsmn} = M^{f}_{rsmn} + M^{p}_{rsmn}$ is the combined mass matrix. The solution of Eq. (35) yields the modal coefficients of the fluid-loaded plate displacement. Substituting these coefficients into Eq. (2), the transversal displacement of the plate is obtained.

2.2. Vibroacoustic indicators

The following vibroacoustic indicators are derived from the formulation that has been presented in the previous section for a baffled thin plate near the free surface of a fluid. Similar expressions for a thin plate in a semiinfinite domain can be obtained from using the Green's function presented in Appendix B.

2.2.1. Vibration response

Vibration response of the plate is evaluated with a calculation of the spatial average of the square of the plate velocity which is given by

$$\left\langle v^2 \right\rangle = \frac{1}{S} \int_S \left| v\left(\mathbf{x_0}, \omega\right) \right|^2 dS, \tag{37}$$

where $S = ab$ is the plate surface area. Substituting the velocity of the plate that is presented in Eq. (13), the expression reduces to [51]

$$\left\langle v^2 \right\rangle = \frac{\omega^2}{4} \sum_{m=1}^{\infty} \sum_{n=1}^{\infty} |W_{mn}(\omega)|^2 . \tag{38}$$

For numerical evaluation of the expression, a truncation to the contribution of plate modes is required. The square of the plate velocity is then expressed as

$$\left\langle v^2 \right\rangle = \frac{\omega^2}{4} \sum_{m=1}^{M} \sum_{n=1}^{N} |W_{mn}(\omega)|^2 . \tag{39}$$

where M, N are the plate modal orders and chosen to be sufficient in the calculation of vibroacoustic indicators within a specified frequency range $[\omega_{\min}, \omega_{\max}]$. The plate modal orders are selected to be the highest modes required for plate responses up to $1.3 \cdot \omega_{\max}$ based on the approximation for the natural frequencies of a fluid-loaded plate [8]

$$\omega_{mn} \approx k_{mn}^2 \sqrt{\frac{D}{\rho_p h}} \left(1 + \frac{\rho_0}{\rho_p h \, k_{mn}}\right)^{-0.5} \tag{40}$$

where $k_{mn} = \sqrt{(m\pi/a)^2 + (n\pi/b)^2}$ are the primary effective wavenumber components of vibration.

2.3. Acoustic response

Pressure at a field point in the fluid is calculated by a similar expression as given in Eq. (28) and using the mode selection criteria from Eq. (40)

$$p(\mathbf{x}, \omega) = \rho_0 \omega^2 \sum_{m=1}^{M} \sum_{n=1}^{N} W_{mn}(\omega) \int_0^b \int_0^a \varphi_{mn}(\mathbf{x_1}) \cdot G(x - x_1, y - y_1, z) \, dx_1 \, dy_1. \tag{41}$$

Radiated sound power can be calculated by integrating the intensity at the surface of the plate. The acoustic power expression is given as [49]

$$\Pi(\omega) = \frac{1}{2} \int_{-\infty}^{\infty} \int_{-\infty}^{\infty} \mathrm{Re}\left\{p_0(\mathbf{x}, \omega) \cdot \bar{v}(x, y)\right\} \, dxdy, \tag{42}$$

where $\bar{}$ denotes the complex conjugate. This expression can be written in terms of pressure and velocity in the wavenumber domain [49]

$$\Pi(\omega) = \frac{1}{8\pi^2} \mathrm{Re}\left\{ \int_{-\infty}^{\infty} \int_{-\infty}^{\infty} p_0^*\left(k_x, k_y, \omega\right) \cdot \bar{v}^*\left(k_x, k_y, \omega\right) dk_x dk_y \right\}. \tag{43}$$

where

$$v^*\left(k_x, k_y, \omega\right) = \mathrm{j}\omega \sum_{m=1}^{M} \sum_{n=1}^{N} W_{mn}(\omega) \, \varphi_{mn}^*\left(k_x, k_y\right), \tag{44}$$

is the Fourier transform of the plate velocity and the Fourier transform of the plate mode shapes function

$$\varphi^*_{mn}\left(k_x, k_y\right) = \int_S e^{i\left(k_x x + k_y y\right)} \varphi_{mn}\left(\mathbf{x}\right) dS \;=\; \sqrt{\frac{2}{ab}}\, I^x_m\left(a\right) I^y_n\left(b\right), \tag{45}$$

with

$$I^p_q\left(r\right) = \begin{cases} \left(\dfrac{q\pi}{r}\right) \dfrac{\left(-1\right)^q e^{\mathrm{j}\left(k_p r\right)} - 1}{k_p^2 - \left(\frac{q\pi}{r}\right)^2}, & k_p \neq \dfrac{q\pi}{r}, \\ \frac{1}{2}\mathrm{j}r & \text{otherwise.} \end{cases} \tag{46}$$

Combining the relations from Eqs. (11), (13), (17) and (18), the acoustic power expression is written as

$$\Pi\left(\omega\right) = \frac{1}{8\pi^2}\mathrm{Re}\left\{\int_{-\infty}^{\infty}\int_{-\infty}^{\infty} \rho_0 \mathrm{j}\omega \left|v^*\left(k_x, k_y\right)\right|^2 \cdot \frac{1}{\gamma}\, \frac{e^{\gamma H} + e^{-\gamma H}}{e^{\gamma H} - e^{-\gamma H}}\, dk_x dk_y \right\}. \tag{47}$$

For computational convenience, the acoustic power is calculated with a change of variables applied such that polar wavenumbers are considered i.e. $k_x = k_r \cos\left(\theta\right)$ and $k_y = k_r \sin\left(\theta\right)$. The expression from Eq. (47) simplifies to

$$\Pi\left(\omega\right) = \int_{\theta=0}^{\theta=2\pi} \int_{k_r=0}^{k_r=\infty} \left|v^*\left(k_r\cos\left(\theta\right), k_r \sin\left(\theta\right)\right)\right|^2 \Theta\left(k_r\right)\; dk_r\, d\theta \tag{48}$$

with

$$\Theta\left(k_r\right) = \begin{cases} \dfrac{\rho_0 \omega k_r}{8\pi^2}\, \mathrm{Re}\left\{ \mathrm{j} \dfrac{\tan\left(\sqrt{k_0'^2 - k_r^2}\, H\right)}{\sqrt{k_0'^2 - k_r^2}} \right\} & \text{for } 0 \leq k_r \leq k_0, \\ \dfrac{\rho_0 \omega k_r}{8\pi^2}\, \mathrm{Re}\left\{ \mathrm{j} \dfrac{\tanh\left(\sqrt{k_r^2 - k_0'^2}\, H\right)}{\sqrt{k_r^2 - k_0'^2}} \right\} & \text{for } k_r > k_0, \end{cases} \tag{49}$$

where it is reminded that k_0' is the complex acoustic wavenumber. Computation is performed numerically with the upper limit of the integral found to be sufficiently truncated to $10^3\; k_0 \;\geq\; 10\; k_f$, where $k_f \approx \sqrt{\omega_{\max}\sqrt{h\rho_p/D}}$ are the plate flexural wavenumbers.

3. Numerical Results

3.1. Model verification

Table 1: Dimensions and material properties of the plate and fluid properties.

Parameter	Value
Young's Modulus E (GPa)	68
Poisson's ratio ν	0.3
Density of plate ρ_s (kg m^{-3})	2740
Density of fluid ρ_0 (kg m^{-3})	1026
Speed of sound c_0 (m s^{-1})	1500
Length a (mm)	600
Width b (mm)	525
Thickness h (mm)	2.4
Structural damping η	0.01
Fluid damping η_f	0.0001

The technique described in this paper is implemented in MATLAB. A convergence study for the analytical model is first performed to investigate the number of terms necessary for the summation term in the Green's function for the waveguide domain as found in Eqs. (25) and (26). The pressure at a point in the fluid domain is used as an indicator for convergence of the results. Pressure spectra in terms of a sound pressure level SPL $= 10 \log_{10} |P/P_0|$, where $P_0 = 1 \times (10)^{-12}$ Pa, is calculated and compared against a reference solution with 500 terms. The difference Δ across an excitation frequency range is evaluated for different truncation numbers and for two different free surface heights. In Fig. 2a, a near free surface of $H = 0.1$ m is applied with a pressure calculated at the midpoint of the centre of the plate to the free surface i.e. $(a/2, b/2, H/2)$. The number of terms required to be within 0.5 dB agreement with the reference solution is observed to occur at 200 terms. In Fig. 2b, a far free surface of $H = 10$ m is applied with a pressure calculated at $(a/2, b/2, H/2)$ as well. The number of terms required to be within 0.5 dB agreement with the reference solution is observed to occur at 25 terms. From these two examples, it can be qualitatively inferred that the further the free surface, the lesser terms necessary for convergence.

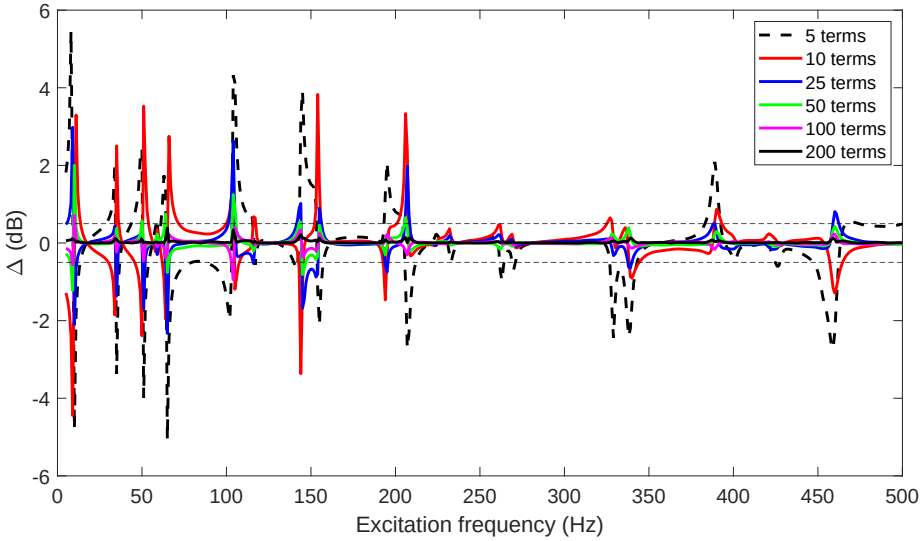

(a)

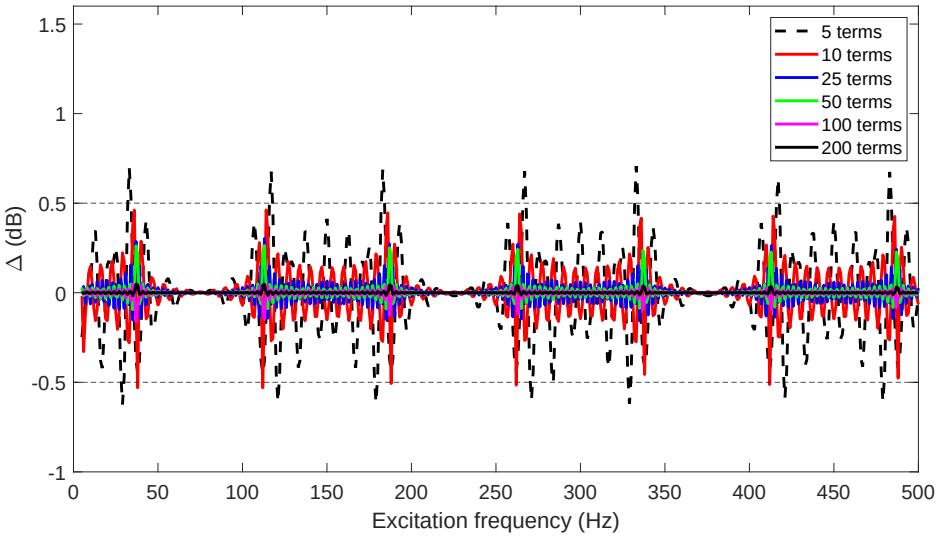

(b)

Figure 2: Convergence study for (a) $H = 0.1$ m and (b) $H = 10$ m. Solutions with 5, 10, 25, 50, 100, and 200 terms are compared against a reference solution using 500 terms (dB ref. 1×10^{-12} Pa).

Preliminary results are initially generated using the same plate and fluid specifications as in Gu and Fuller's investigation [8]. The analytical model was able to successfully reproduce the relevant vibration results in a semiinfinite heavy fluid domain using a formulation similar to the present study shown in Fig. 3. The necessary adjustments to the present formulation are summarized in Appendix B.

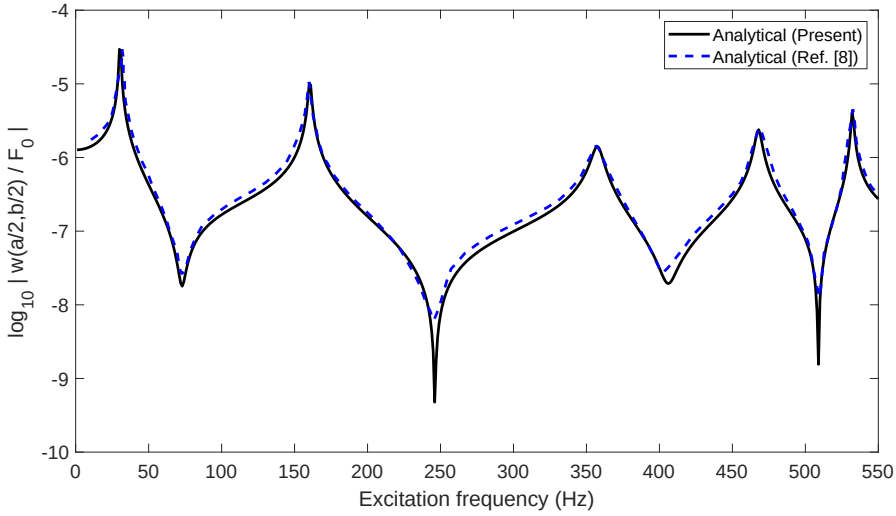

Figure 3: Plate center-point displacement for a fluid-loaded plate in a semiinfinite domain (dB ref. 1 mN^{-1}).

To verify the code, the analytical results are compared with a 3D finite element model of a fully coupled fluid-structure system which is developed using the commercial software COMSOL Multiphysics (v5.5). The plate and fluid specifications are summarized in Tab. 1 and the magnitude of the force is $F_0 = 10$ N applied at the centre of the plate $(a/2, b/2, 0)$. Fig. 4 shows a schematic diagram of the plate model coupled with a finite layer of water. Since the force was applied at the centre of the plate, it is not necessary to model the full computational domain in the finite element model. A symmetry boundary condition was applied at the side boundaries of the quarter finite element domain for both fluid and structure as shown in Fig. 4. A perfectly matched layer (PML) was applied on the boundary of the computational domain and appropriately tuned to allow the outgoing waves to leave the domain with minimal reflections. This is a challenge for the finite element method as the acoustic wavelengths are quite large at low frequencies in water. Therefore a relatively large PML is required to achieve satisfactory results, particularly at low frequencies. The boundaries of the computational domain in the finite element model was discretised using

the quadratic quadrilateral elements and a 3D structured mesh was created by sweeping the 2D mesh from the boundary. A fine mesh was used for all the numerical models to ensure accurate numerical predictions. The largest element size was less than 1/10 the wavelength at the highest frequency considered in this work. The fluid was modelled using the COMSOL Pressure Acoustics module, and the plate was modelled as a linear elastic medium using the Solid Mechanics module. The Acoustic-Structure boundary condition was used to couple the pressure acoustics model (fluid) to the structural component (plate). The numerical computations were performed in the frequency domain to find the response of the fully coupled fluid-plate system subjected to harmonic force excitation.

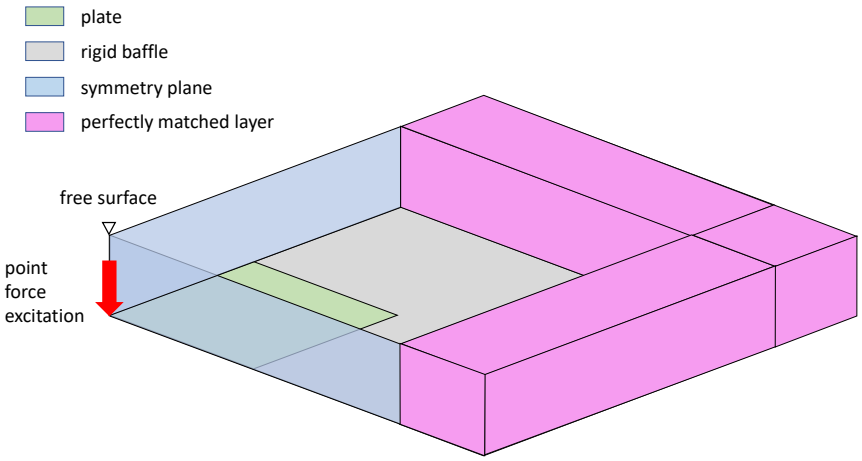

Figure 4: Schematic diagram of the COMSOL model.

Model verification is then performed by generating the results for the two limiting cases of a free surface, which includes the in-vacuo plate response and heavy fluid loading response in a semiinfinite fluid domain, as shown in Fig. 5. Results show the vibration response, which is characterized by the mean quadratic velocity which is calculated using Eq. (39). The analytical results are verified against corresponding results using a COMSOL model and agree very well (the in-vacuo plate result from COMSOL is not shown here). When comparing the two limiting cases, the well-known added mass effect associated with heavy fluid loading [35, 8] is observed and there is a shift of the in-vacuo natural frequencies towards the lower frequencies. Vibroacoustic responses of a plate near a free surface is also predicted and verified against a corresponding COMSOL model, where a plate near a free surface of $H = 0.1$ m is chosen as the case study. Vibration

response of the plate is shown in Fig. 6, and for the acoustic response, acoustic power and field pressure is evaluated. Acoustic power is predicted using Eq. (48), and presented in Fig. 7. Acoustic pressure is evaluated using Eq. (41) at various locations in the fluid domain (results not shown here). It is found that these vibroacoustic results agree very well with the COMSOL model. Further verification has been performed that demonstrate the convergence of the plate response with a far free surface to the response of a plate in a semiinfinite fluid domain as shown in Fig. 8, where the acoustic power for a fluid-loaded plate with a very far free surface converges to the result of the acoustic power for a fluid-loaded plate in a semiinfinite fluid domain.

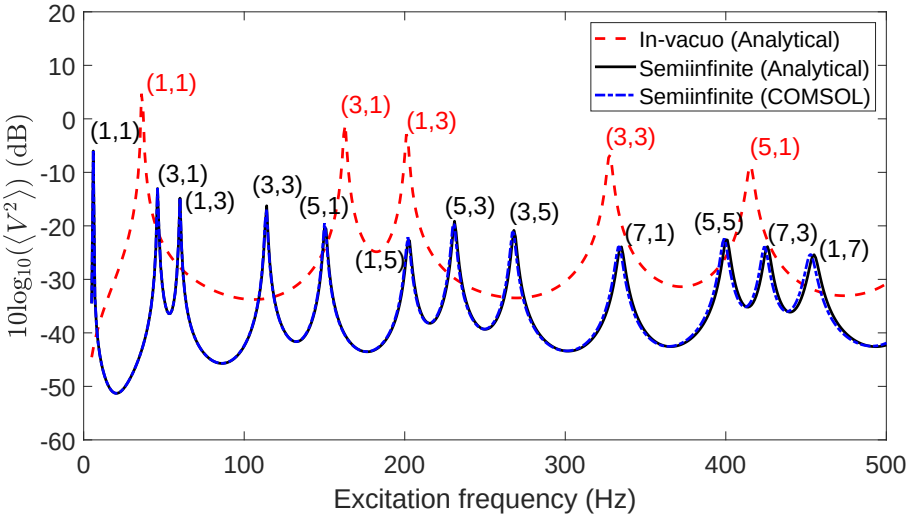

Figure 5: Mean quadratic velocity spectra of an in-vacuo plate and fluid-loaded plate in semiinfinite domain under point force excitation, where resonant mode types are labelled as (m,n) (dB ref. 1 $\mathrm{m^2 s^{-2} Hz^{-1}}$).

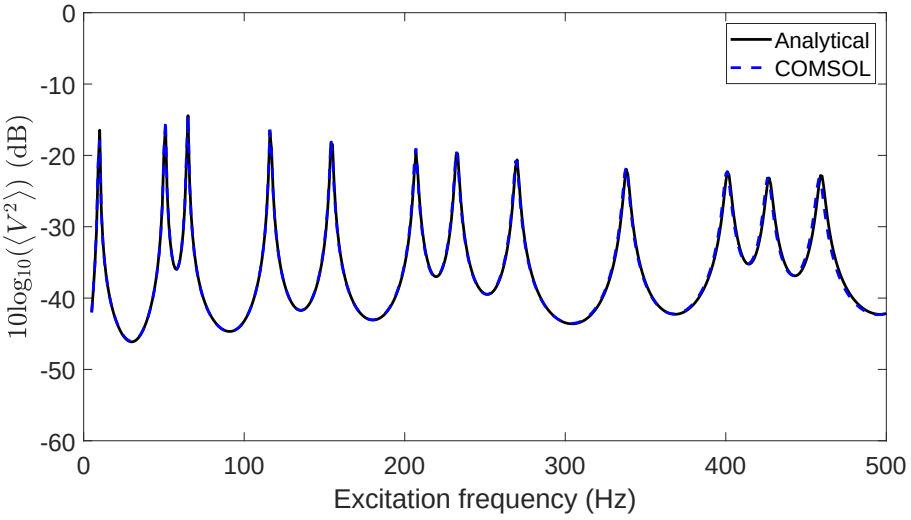

Figure 6: Mean quadratic velocity spectra of the fluid-loaded plate near a free surface (H = 0.1 m) (dB ref. 1 $m^2s^{-2}Hz^{-1}$)

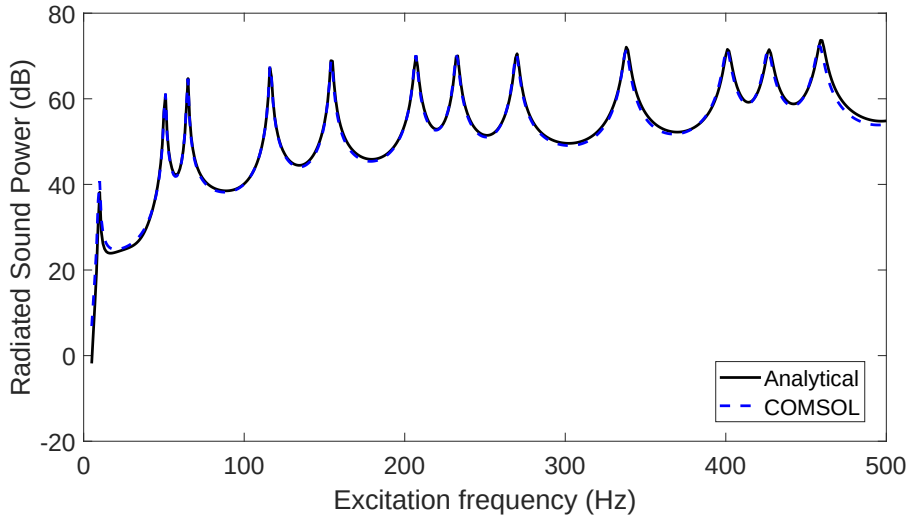

Figure 7: Predicted acoustic power of a fluid-loaded plate near a free surface (H = 0.1 m) (dB ref. 1×10^{-12} W).

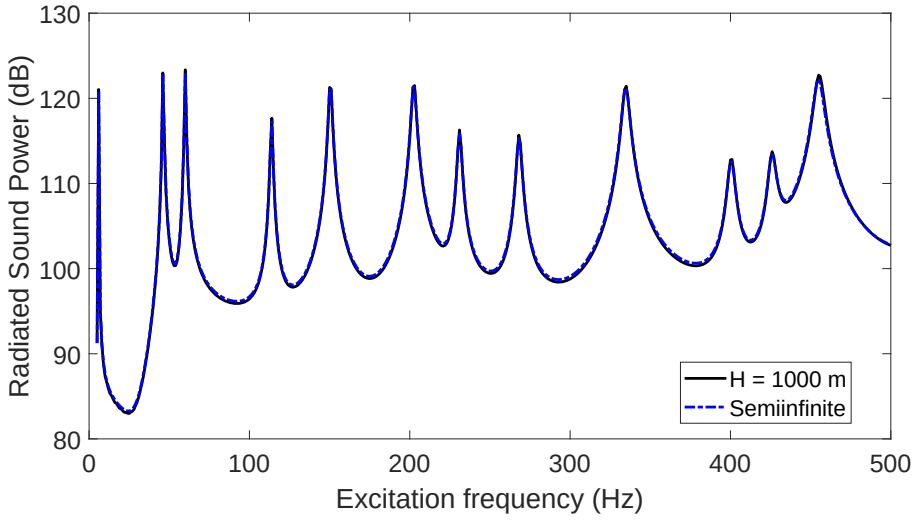

Figure 8: Predicted acoustic power of a plate in an acoustic domain with a very far free surface (H = 1000m), and in a semiinfinite domain (dB ref. 1×10^{-12} W).

3.2. Added mass effect

The vibration and acoustic results from a plate in a semiinfinite domain compared against results from a plate near a free surface are considerable different. Therefore, it is suggestive that the height of the free surface has a significant effect on the plate response. To evaluate the trend between the height of the free surface and plate response, predictions of the vibration response are evaluated at various free surface heights and compared against a reference case of a plate with a free surface of $H = 0.1$ m. The height of the free surface is decreased from the reference case in Fig. 9a. It is observed that decreasing the height of the free surface results in the natural frequencies of the plate to shift towards higher frequencies and towards the in-vacuo plate modes due to a decrease of the fluid volume above the plate from the added mass effect [39, 52, 14]. Conversely, when the height of the free surface is increased from the reference case, the spectra converges to the semiinfinite case as shown in Fig. 9b. It is noticed that the low frequency resonant peak amplitude remains smaller when comparing a plate with $H = 1$ m to a plate with a semiinfinite domain. This can be explained by the height of the free surface restricting the possible wavelengths to be exhibited in the waveguide domain. The low frequency amplitude has been observed to converge at a sufficiently far free surface.

To explicitly investigate the added mass effect, an analytical matrix expression for the added mass ratio is

presented with the assumption of an incompressible fluid. The computation of the added mass ratio involves taking the added mass component from the fluid loading impedance in Eq. (30) and presenting it as a ratio to the plate mass

$$\frac{M^f_{rsmn}}{M^p_{rsmn}} = \begin{cases} \Gamma(m,n) = \mathrm{Re}\left\{ \dfrac{16\rho_0 ab}{\rho_p h} \displaystyle\int_0^1 \int_0^1 \Phi_{rm}(u)\, \Phi_{sn}(v)\, \Omega(u,v)\,|_{k_0=0}\; du\, dv \right\} & \text{for } r = m \wedge s = n, \\ 0 & \text{otherwise,} \end{cases} \tag{50}$$

where $\Gamma(m,n)$ is the added mass ratio for a given element or plate mode (m,n), and the acoustic wavenumber is set to zero ($k_0 = 0$) for an incompressible fluid. This is equivalent to solving the Laplace equation instead of the Helmholtz equation in Eq. (14). The added mass ratio is investigated for the first five plate modes in Fig. 10. The effect of the free surface can be observed to significantly alter the added mass effect across the plate modes. For a sufficiently near free surface, all five plate modes have a relatively low and similar added mass ratio. As the free surface height is increased, the added mass ratios across all five plate modes increase due to the increase in fluid volume above the plate until a free surface height becomes sufficiently far so that the added mass ratio converges to that of a plate in a semiinfinite domain. Higher plate modes are observed to converge to the added mass ratio for a plate in a semiinfinite domain at lower free surface heights.

The natural frequency of the fluid-loaded plate modes can be calculated using the added mass ratio and in-vacuo plate modes with the following relation [53]

$$\omega_{mn,\mathrm{f}} = \frac{\omega_{mn,\mathrm{v}}}{\sqrt{\Gamma(m,n)+1}}, \tag{51}$$

where $\omega_{mn,\mathrm{v}} = k_{mn}\sqrt{D/\left(\rho_p h\right)}$ is the natural frequency for an in-vacuo plate mode, and $\omega_{mn,\mathrm{f}}$ is the natural frequency of a plate mode subjected to fluid loading and with a free surface. Using this expression, the natural frequencies of the first five plate modes can be computed by evaluating the added mass ratios using Eq. 50. For a plate near a free surface of $H = 0.1$ m, the first five natural frequencies of the plate are calculated and compared against corresponding values from Fig. 6, and are presented in Tab. 2 in Hz i.e. $f = \dfrac{\omega}{2\pi}$. Considering that the figure has a resolution of 1 Hz, the results are shown to be in very good agreement.

Table 2: First five natural frequencies of the plate

Mode	$\Gamma(m,n)$	$f_{mn,\mathrm{v}}$ (Hz)	$f^{a}_{mn,\mathrm{f}}$ (Hz)	$f^{b}_{mn,\mathrm{f}}$ (Hz)
$(1,1)$	13.4	36.4	9.59	10
$(3,1)$	9.31	163	50.7	51
$(1,3)$	8.67	201	64.7	65
$(3,3)$	6.93	328	116	117
$(5,1)$	6.26	415	154	154

[a] calculation via analytical expressions;

[b] from the Mean quadratic velocity spectra in Fig. 6.

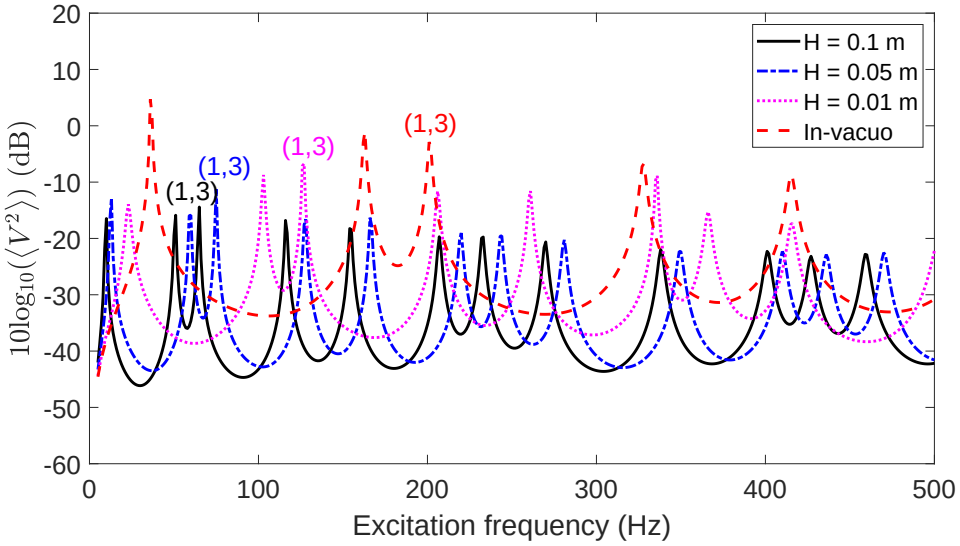

(a)

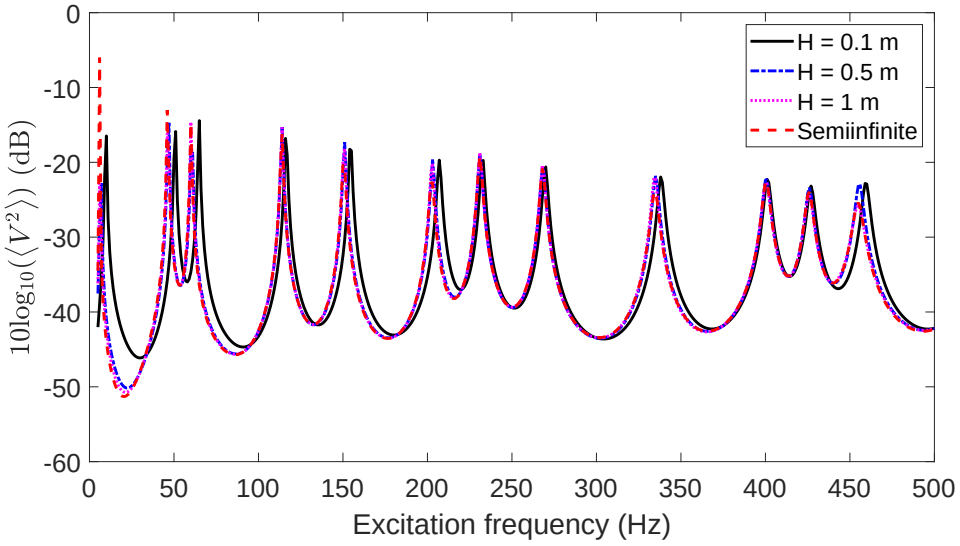

(b)

Figure 9: Predicted mean quadratic velocity spectra of plate with a free surface compared against (a) lower free surfaces and (b) higher free surfaces (dB ref. 1 $m^2s^{-2}Hz^{-1}$).

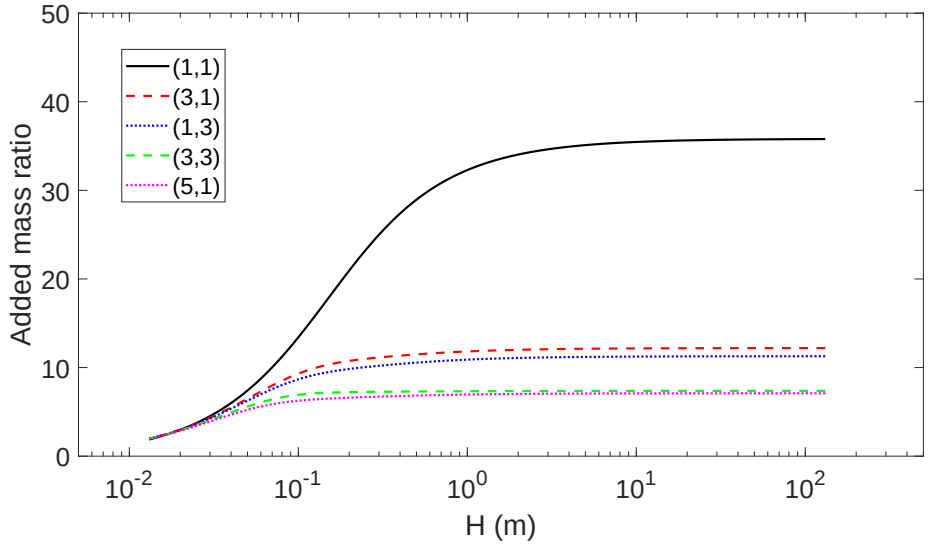

Figure 10: Added mass ratio for the first five plate modes.

3.3. Standing waves criterion

The expression for the spectral velocity potential from Eq. (18) becomes unbounded when fluid damping is not considered. A specific condition arises which is referred to as the standing waves criterion, where, for a given height of a free surface and at certain excitation frequencies, the outgoing acoustic waves form a standing wave between the baffled plate and free surface. In this section, an investigation into the effect of the standing waves criterion on the vibroacoustic response of a plate is performed. It is reminded that the frequencies for the standing waves are given by

$$f_N = \frac{c_0}{4H}\,(2N+1) \;\text{ with } N = 0, 1, 2, 3... \tag{52}$$

or when an odd integer multiple of a quarter wavelength of the acoustic waves matches the height of the free surface i.e. $\lambda_N/4 = H/\,(2N+1)$, where λ is the acoustic wavelength. The standing waves criterion manifests at low to medium frequency range for a far free surface. A case study is then selected for a plate with a far free surface of $H = 10$ m, such that the excitation frequencies that satisfy the standing waves criterion are present in the frequency range of interest [5 Hz, 500 Hz].

Acoustic pressure is predicted for the case study at an observation point $(a/2, b/2, H/2)$, and the result is compared against the analytical result for a plate in a semiinfinite fluid domain. It is first recognized that

the general shape of the two pressure spectra are in reasonable agreement, suggesting that the free surface is far enough so that the added mass effect from a free surface is negligible. However, at certain excitation frequencies, aside from the plate resonant peaks, the standing waves criterion present secondary peaks that are highlighted in the figure. Some peaks are non-existent, such as for $N = 1, 2$ and 4. This is due to the spectral proximity to the plate resonance, which dominates the spectra. Generally, the effect is not significant and this is due to the waveguide domain allowing the acoustic energy at the standing wave frequencies to propagate in the $x-$ and $y-$ directions to infinity. The pressure is then presented in the acoustic domain in the $y - z$ plane for excitation frequencies that satisfy the standing waves criterion at $N = 3$ and $N = 6$, in Figs. 12a and 12b respectively, for a non-resonant frequency in Fig. 12c, and a resonant plate frequency in Fig. 12d. For Figs. 12a and 12b, the excitation frequencies satisfy the standing waves criterion, and the presence of a standing wave is observed. The wavelengths of the standing waves are evaluated by using Eq. 52. For Figs. 12c and 12d, there is no consistent constructive and destructive interference of the acoustic waves between the free surface and baffled plate. As a result, there are no standing waves formed.

As shown in Fig. 13, the pressure in the far field from the plate is also studied by considering an observation point $(a/2 + x', b/2, H/2)$, with $x' = 10$ m and $x' = 100$ m. The results are compared to an observation point directly above the plate, corresponding to $x' = 0$ m. Comparing the pressure at frequencies below the first standing wave ($N = 0$) frequency, it is observed that there is a decrease of approximately 20 dB and the acoustic waves behave with spherical-like propagation i.e. $P_{x'=10}/P_{x'=100} = 1/R$. For frequencies above the first standing wave frequency, there is a decrease of approximately 10 dB and acoustic waves are observed to behave with cylindrical-like propagation i.e. $P_{x'=10}/P_{x'=100} = 1/\sqrt{R}$. It can then be inferred that the plate is more efficient in far field radiation for frequencies above the standing wave frequency. This is shown to be the case in Fig. 15b where the radiated sound power for a plate with a free surface of $H = 10$ m is evaluated.

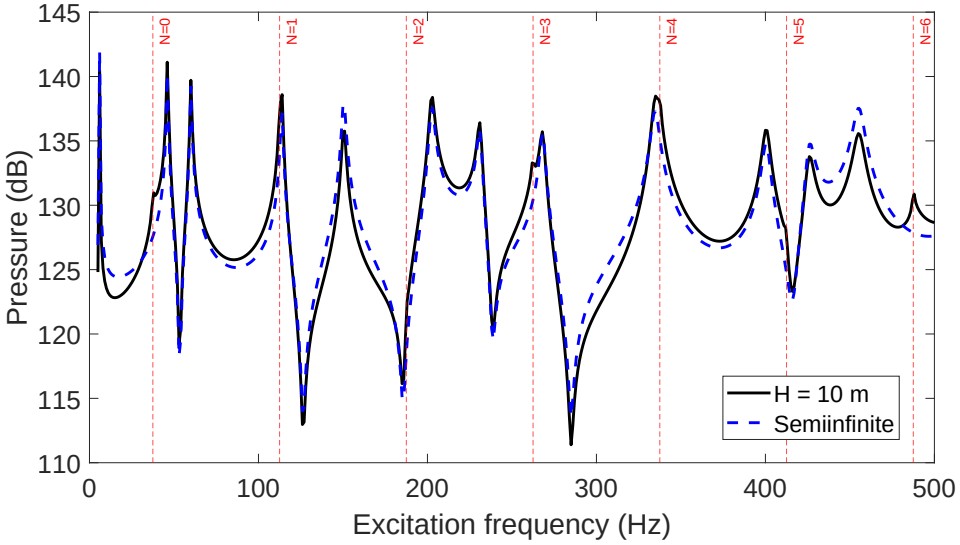

Figure 11: Pressure spectra for a plate in an acoustic domain with a far free surface ($H = 10$ m), and in a semiinfinite domain at an observation point of $(a/2, b/2, H/2)$ (dB ref. 1×10^{-12} Pa).

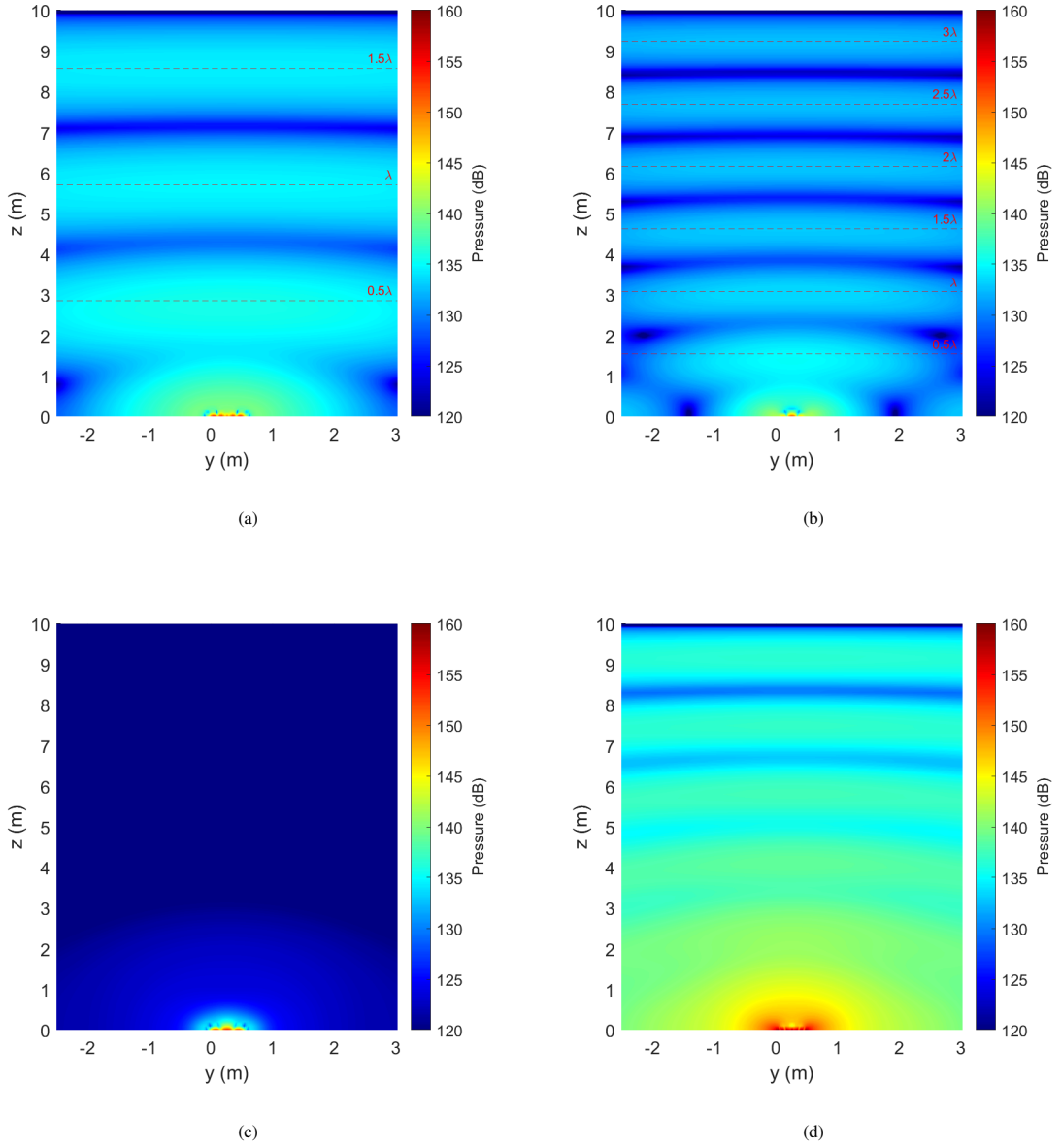

Figure 12: Acoustic pressure from the surface of the plate to the height of the free surface (H = 10 m) for excitation frequencies of (a) 262.5 Hz, (b) 487.5 Hz, (c) 239 Hz, and (d) 455 Hz. The standing waves criterion is satisfied for (a) and (b), with an acoustic wavelength of $\lambda \approx 5.71$ m and $\lambda \approx 3.08$ m respectively, represented by - - - - -. The excitation frequency of (c) and (d) are at non-resonant and resonant plate frequencies respectively (dB ref. 1×10^{-12} Pa).

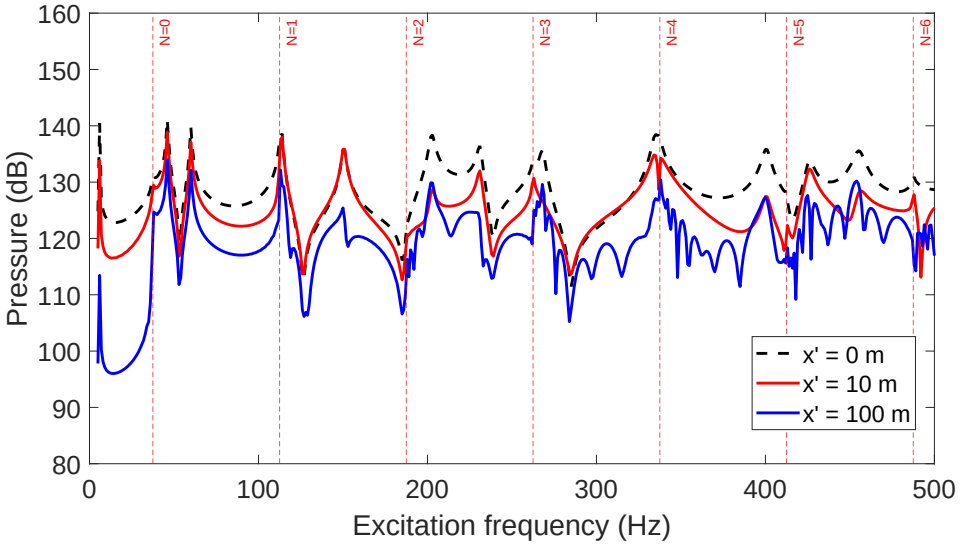

Figure 13: Pressure spectrum for a plate in an acoustic domain with a far free surface ($H = 10$ m) at an observation point of $(a/2 + x', b/2, H/2)$ (dB ref. 1×10^{-12} Pa).

3.4. Wavenumber contribution to acoustic power

Prediction of the acoustic power from Eq. (48) presents an integral that can be divided into two domains of the acoustic radiation circle: the supersonic region where the wavenumbers are less than the acoustic wavenumber and inside the acoustic radiation circle, and the subsonic region where the wavenumbers are greater than the acoustic wavenumber and outside the acoustic radiation circle. The effect of a free surface on the power contribution of these regions to the total acoustic power is investigated. Maps are generated in Fig. 14, that show the magnitude of the components of the integrand in Eq. (48) across a frequency range of $[5\text{ Hz}, 500\text{ Hz}]$. The integrand consists of the square of the plate velocity in the wavenumber domain $\left|v\left(k_x, k_y\right)\right|^2$ and $\Theta\left(k_r\right)$, where k_r is the polar wavenumber. A dynamic range of 100 dB is maintained across all the figures and two cases are considered, a plate near free surface of $H = 0.1$ m, and a plate with a far free surface of $H = 10$ m. The wavenumbers are considered for $k_y = 0$ i.e. $k_r = k_x$.

In Figs. 14a and 14b, maps of $\left|v\left(k_x, k_y\right)\right|^2$ for the two plate cases are presented. The plate modes are observed as resonant striations within the frequency range. When comparing the maps, there is a very slight shift of the plate modes between the $H = 0.1$ m case and $H = 10$ m case. The difference in natural frequencies between the two plate cases is due to the different fluid volume above the plate, as shown in

Fig. 9b, where a plate with a free surface of $H = 10$ m can be considered to be approximately a plate in a semiinfinite domain. In Figs. 14c and 14d, the function $\Theta(k_r)$ is evaluated. When compared between the two plate caes, the maps are observed to be very dissimilar.

The integrand is then investigated by taking the product of the two components and normalized across k_x for each excitation frequency in Figs. 14e and 14f. In these maps, it is observed that there is significant contribution outside the radiation circle for a near free surface of $H = 0.1$ m, while for a far free surface of $H = 10$ m, there is a significant contribution at low frequencies below the $N = 0$ standing wave frequency i.e. for acoustic quarter-wavelengths greater than H. For a near free surface, the contribution from outside the radiation circle is significant to at least the order of the plate flexural wavenumbers, suggesting the integrand should be evaluated beyond the radiation circle. At low excitation frequencies, the contribution from outside the acoustic circle extends to approximately $10^3\ k_0$. While at higher frequencies, the contribution from outside the acoustic circle extends to approximately $10^2\ k_0$. Comparatively, for a far free surface, the contribution from outside the radiation circle is virtually insignificant for excitation frequencies above the $N = 0$ standing wave frequency, and all of the contribution from the integrand occurs inside the acoustic radiation circle. It is also observed in Figs. 14d and 14f, the presence of curved striations below the acoustic wavenumber which present where the standing waves criterion is satisfied from Eq. (52) i.e. $k_z = \sqrt{k_0^2 - k_r^2} = \pi(2N + 1)/(2H)$. From the comparison of these maps, it is suggestive that the wavenumbers from outside the acoustic circle (i.e. the subsonic region) is significantly more contributing in the total power than the wavenumbers from inside the acoustic circle (i.e. the supersonic region) for a plate near a free surface. The inverse can be implied for a far free surface, where the supersonic region is of significant contribution to total power compared to the subsonic region for excitation frequencies above the $N = 0$ standing wave frequency.

Acoustic power is then investigated for the two plate cases in Fig. 15, where the integral from Eq. (48) is evaluated numerically. The supersonic region is evaluated by taking the integral limits between $k_r = 0$ and $k_r = k_0$, and the subsonic region is evaluated by taking the limits between $k_r = k_0$ and $k_r = 10^3\ k_0 \geq 10^2\ k_f$. Taking the sum of the two evaluates the total power. For a free surface of $H = 0.1$ m in Fig. 15a, the total power is shown to be dominated by the subsonic region whereas for a free surface of $H = 10$ m in Fig. 15b, the total power is dominated by the supersonic region for excitation frequencies above the $N = 0$ standing wave frequency, and dominated by the subsonic region below this frequency. In the case of a very far free surface ($H = 100$ m), the $N = 0$ standing wave frequency is 3.75 Hz, and the total power across the excitation frequency range of [5 Hz, 500 Hz] is entirely dominated by the supersonic (results are not shown here).

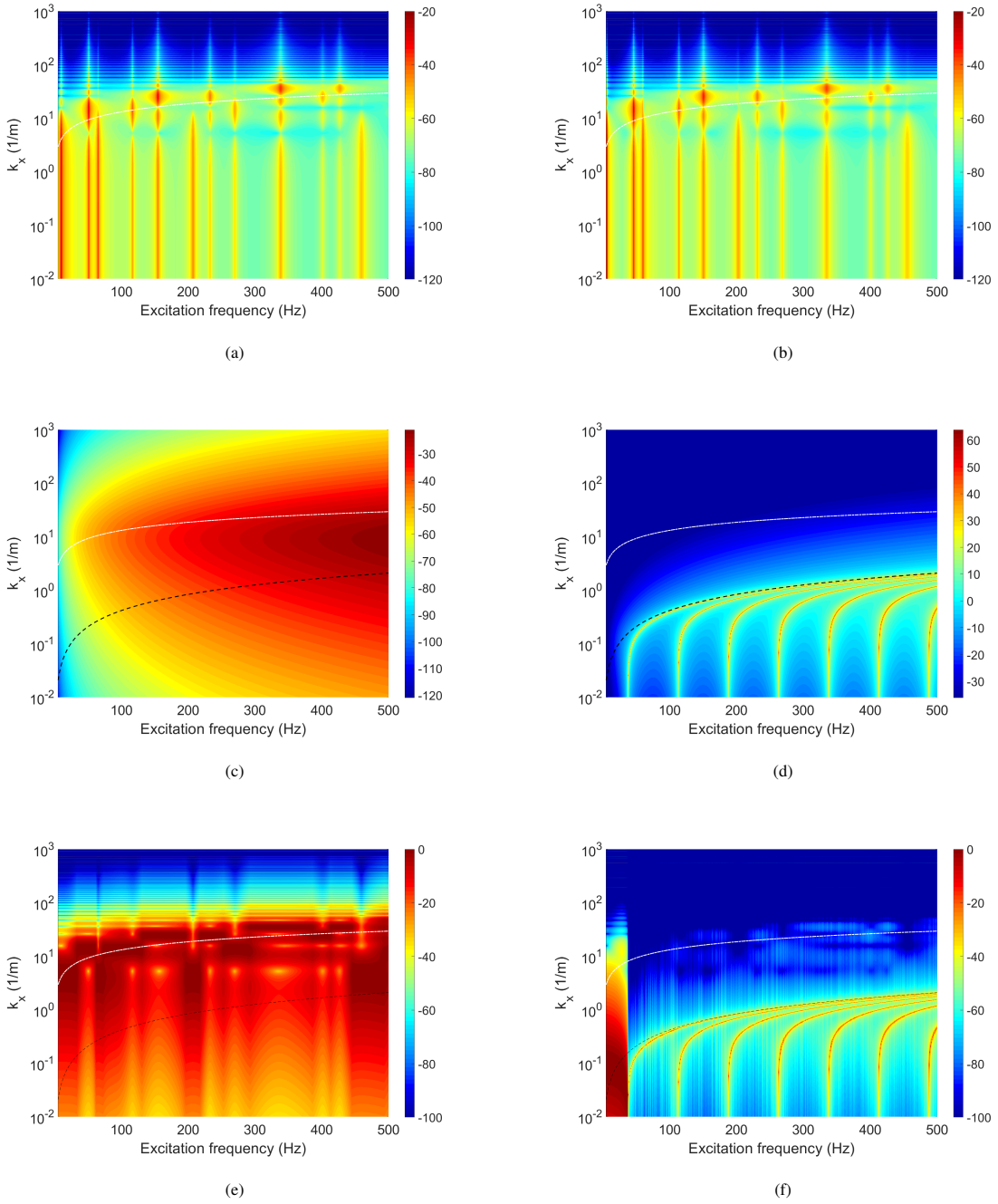

Figure 14: Maps for a free surface of $H = 0.1$ m (left) and $H = 10$ m (right) of: (a,b) $|v^*(k_x, 0)|^2$ (dB ref. 1 $\mathrm{m^6 s^{-2}}$), (c,d) $\Theta(k_x)$ (dB ref. 1 $\mathrm{kgm^{-3}\ s^{-1}}$), and (e,f) $|v^*(k_x, 0)|^2 \cdot \Theta(k_x)$ normalized by the maximum value at each excitation frequency (dB ref.1 $\mathrm{kgm^{-3} s^{-3}}$). The white dashed-dot line in (a,b) corresponds to the plate flexural wavenumber; the black dashed line in (c,d) and (e,f) corresponds to the acoustic wavenumber.

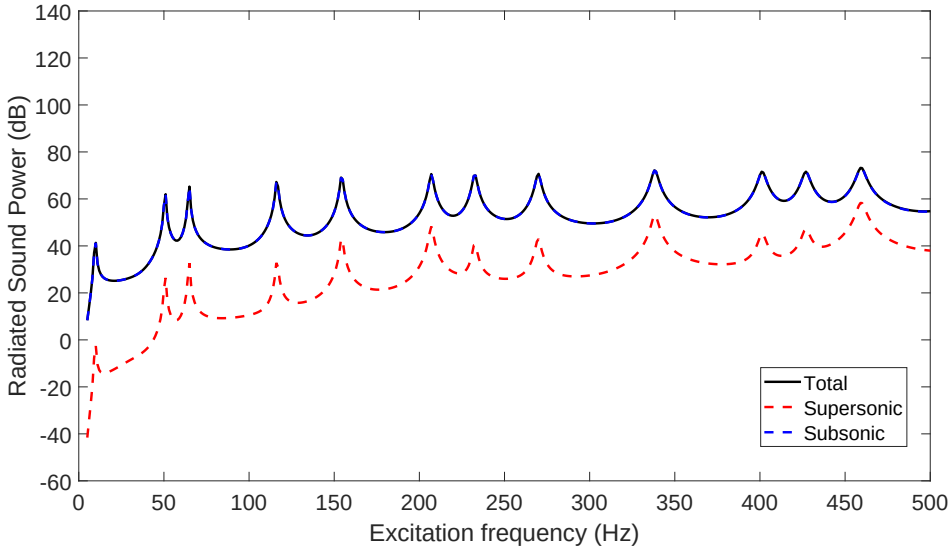

(a)

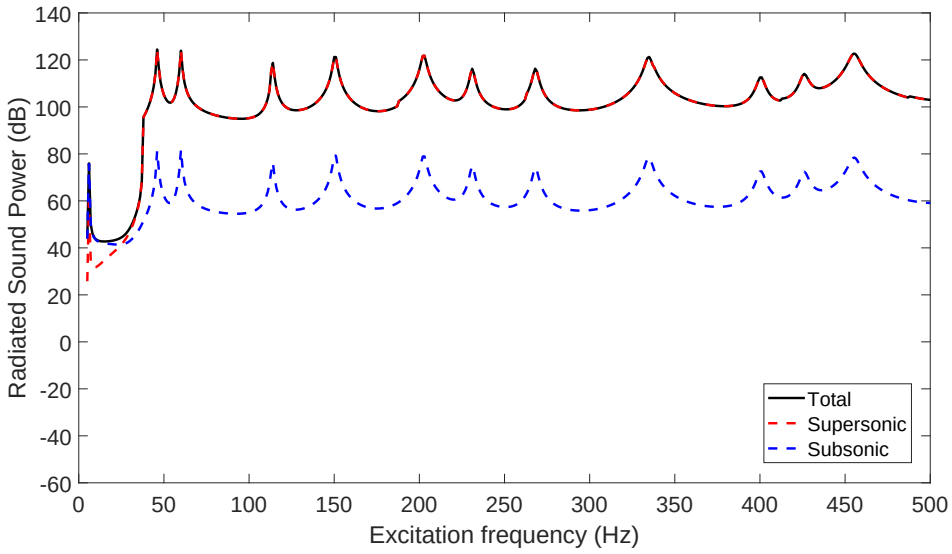

(b)

Figure 15: Acoustic power contribution for a free surface at (a) $H = 0.1$ m and (b) $H = 10$ m (dB ref. 1×10^{-12} W).

4. Conclusions

An analytical approach for the forced vibroacoustic response of a baffled rectangular thin plate near a free surface of a fluid was herein presented. The transversal displacement of the plate was decomposed on the basis of the in-vacuo plate modes and formed the basis for the Fourier decomposition of the fluid loading. This approach extended Sandman's formulation [35], which originally focused on a thin plate immersed in a semiinfinite domain. With the inclusion of a free surface, the analytical model presented a novel approach for predicting the vibroacoustic indicators that characterize the forced response of the plate and have been verified against finite element simulations using COMSOL. Significant effects of a free surface on the vibroacoustic behavior of the baffled plate were observed. From the present model, the added mass effect was demonstrated. The natural frequencies of a plate near a free surface converges to the plate modes of an in-vacuo plate. While the natural frequencies of a plate with a sufficiently far free surface converges to the plate modes in a semiinfinite domain. An analytical expression for the added mass ratio that accounts for the variation in the height of a free surface was also presented, and through its computation, it was observed that there was a significant change in the fluid-loaded added mass effect for a plate near a free surface. The added mass ratio across the first five plate modes was found to be approximately the same for a near free surface and converges to that of a plate in a semiinfinite domain at a sufficiently far free surface with higher plate modes converging at a lower free surface.

As a consequence of including a free surface, the standing waves criterion emerges in which at certain heights and excitation frequencies there is a small increase in acoustic pressure within the fluid domain. The manifestation of the standing waves can be observed to slightly alter the acoustic pressure response by an addition of secondary peaks at the satisfied excitation frequencies. Additionally, the presence of a free surface was observed to have a significant effect on the acoustic power radiated from the excited plate. It was shown that the relative power contributions from the wavenumbers in the subsonic region and supersonic region of the radiation circle to the total acoustic power were directly affected by the height of the free surface. The subsonic region dominates the total power for frequencies below the $N = 0$ standing wave frequency and conversely the supersonic region dominates above this particular frequency.

Acknowledgements

The first author acknowledges that this research is supported by an Australian Government Research Training Program Scholarship. The second author gratefully acknowledges the financial support by the

Australian Government through the Australian Research Councils Discovery Early Career Project funding scheme (project DE190101412).

Appendix A

$$k_z' = \begin{cases} \kappa_1 - \kappa_2 \mathrm{j} & \text{for } \gamma^2 < 0 \\ \kappa_1 + \kappa_2 \mathrm{j} & \text{for } \gamma^2 > 0. \end{cases} \tag{A.1}$$

where

$$\kappa_1 \approx \sqrt{\frac{k_z^2 + \sqrt{k_z^4 + 4\eta_f^2 k_0^4}}{2}}, \tag{A.2}$$

$$\kappa_2 \approx \sqrt{\frac{-k_z^2 + \sqrt{k_z^4 + 4\eta_f^2 k_0^4}}{2}}, \tag{A.3}$$

assuming η_f^2 is negligible, and $k_z = \sqrt{k_0^2 - k_x^2 - k_y^2}$ for $\gamma^2 < 0$ and $k_z = \sqrt{k_x^2 + k_y^2 - k_0^2}$ for $\gamma^2 > 0$.

Appendix B

Fig. C.1 shows an elastic rectangular thin baffled plate that is simply supported on its four edges and excited by a point force. The infinite baffle is a rigid boundary condition and the fluid domain is unbounded i.e. a semiinfinite domain.

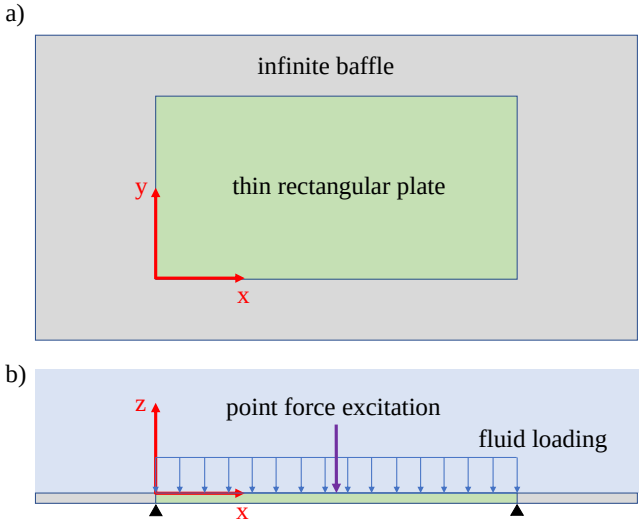

Figure C.1: a) Top view and b) side view of a fluid-loaded baffled plate under point force excitation.

Applying Eqs. (12) - (17) with the Sommerfeld radiation condition

$$\lim_{r\to\infty} r\left(\frac{\partial\Psi}{\partial r} + \mathrm{j}k_0\Psi\right) = 0 \tag{C.1}$$

instead of the pressure release condition of a free surface, the velocity potential solution to the Helmholtz equation is

$$\Psi(\mathbf{x},\omega) = \mathrm{j}\omega \sum_{m=1}^{\infty}\sum_{n=1}^{\infty} W_{mn} \int_0^b \int_0^a \varphi_{mn}(\mathbf{x_1})\, G_{\mathrm{SI}}(x-x_1, y-y_1, z)\ \mathrm{d}x_1\mathrm{d}y_1, \tag{C.2}$$

$$G_{\mathrm{SI}}(x-x_1, y-y_1, z) = \frac{1}{2\pi}\frac{e^{-\mathrm{j}k_0' R}}{R}, \tag{C.3}$$

where G_{SI} is the Neumann Green's function [49] for the semiinfinite domain.

References

[1] M. S. Howe, Acoustics of fluid-structure interactions, Cambridge monographs on mechanics, Cambridge University Press, 1998, https://doi.org/10.1017/CBO9780511662898.

[2] D. Innes, D. Crighton, Power radiated by an infinite plate subject to fluid loading and line drive, J. Sound Vib. 123 (3) (1988) 437–450, https://doi.org/10.1016/S0022-460X(88)80161-5.

[3] Z. Cheng, J. Fan, B. Wang, W. Tang, Radiation efficiency of submerged rectangular plates, Appl. Acoust. 73 (2) (2012) 150–157, https://doi.org/10.1016/j.apacoust.2011.06.017.

[4] B. E. Sandman, J. E. Boisvert, Simplified structural acoustic characterization of external compliant coatings on submerged surfaces, Struct. Acoust. (1995) 65–71.

[5] O. Foin, A. Berry, J. Szabo, Acoustic radiation from an elastic baffled rectangular plate covered by a decoupling coating and immersed in a heavy acoustic fluid, J. Acoust. Soc. Am. 107 (5) (2000) 2501–2510, https://doi.org/10.1121/1.428638.

[6] B. Laulagnet, J. L. Guyader, Sound radiation from a finite cylindrical shell covered with a compliant layer, J. Vib. Acoust. 113 (2) (1991) 267–272, https://doi.org/10.1115/1.2930180.

[7] M. Tao, W. L. Tang, H. X. Hua, Noise reduction analysis of an underwater decoupling layer, J. Vib. Acoust. 132 (6) (2010) 061006, https://doi.org/10.1115/1.4002126.

[8] Y. Gu, C. R. Fuller, Active control of sound radiation from a fluid-loaded rectangular uniform plate, J. Acoust. Soc. Am. 93 (1) (1993) 337–345, https://doi.org/10.1121/1.405668.

[9] B. J. Brévart, C. R. Fuller, Active control of coupled wave propagation in fluid-filled elastic cylindrical shells, J. Acoust. Soc. Am. 94 (3) (1993) 1467–1475, https://doi.org/10.1121/1.408149.

[10] S. Li, Active modal control simulation of vibro-acoustic response of a fluid-loaded plate, J. Sound Vib. 330 (23) (2011) 5545–5557, https://doi.org/10.1016/j.jsv.2011.07.001.

[11] M. Amabili, Effect of finite fluid depth on the hydroelastic vibrations of circular and annular plates, J Sound Vib. 193 (4) (1996) 909–925, https://doi.org/10.1006/jsvi.1996.0322.

[12] M. Kwak, S.-B. Han, Effect of fluid depth on the hydroelastic vibration of free-edge circular plate, J. Sound Vib. 230 (1) (2000) 171–185, https://doi.org/10.1006/jsvi.1999.2608.

[13] E. Askari, K.-H. Jeong, Hydroelastic vibration of a cantilever cylindrical shell partially submerged in a liquid, Ocean Eng. 37 (11-12) (2010) 1027–1035, https://doi.org/10.1016/j.oceaneng.2010.03.016.

[14] E. Askari, K.-H. Jeong, M. Amabili, Hydroelastic vibration of circular plates immersed in a liquid-filled container with free surface, J. Sound Vib. 332 (12) (2013) 3064–3085, https://doi.org/10.1016/j.jsv.2013.01.007.

[15] A. Ergin, B. Uğurlu, Linear vibration analysis of cantilever plates partially submerged in fluid, J. Fluids Struct. 17 (7) (2003) 927–939, https://doi.org/10.1016/S0889-9746(03)00050-1.

[16] Y. Kerboua, A. Lakis, M. Thomas, L. Marcouiller, Vibration analysis of rectangular plates coupled with fluid, Appl. Mathem. Model. 32 (12) (2008) 2570–2586, https://doi.org/10.1016/j.apm.2007.09.004.

[17] S. Hosseini-Hashemi, M. Karimi, H. Rokni, Natural frequencies of rectangular mindlin plates coupled with stationary fluid, Appl. Math. Model. 36 (2) (2012) 764–778, https://doi.org/10.1016/j.apm.2011.07.007.

[18] D. S. Cho, B. H. Kim, N. Vladimir, T. M. Choi, Natural vibration analysis of rectangular bottom plate structures in contact with fluid, Ocean Eng. 103 (2015) 171–179, https://doi.org/10.1016/j.oceaneng.2015.04.078.

[19] S. Soni, N. K. Jain, P. V. Joshi, Analytical modeling for nonlinear vibration analysis of partially cracked thin magneto-electro-elastic plate coupled with fluid, Nonlinear Dyn. 90 (1) (2017) 137–170, https://doi.org/10.1007/s11071-017-3652-5.

[20] S. Soni, N. Jain, P. Joshi, Vibration analysis of partially cracked plate submerged in fluid, J. Sound Vib. 412 (2018) 28–57, https://doi.org/10.1016/j.jsv.2017.09.016.

[21] S. Soni, N. Jain, P. Joshi, A. Gupta, Effect of thermal environment on vibration response of partially cracked functionally graded plate coupled with fluid, Materials Today: Proceedings 5 (14) (2018) 27810–27819, https://doi.org/10.1016/j.matpr.2018.10.017.

[22] K. Khorshid, S. Farhadi, Free vibration analysis of a laminated composite rectangular plate in contact with a bounded fluid, Compos. Struct. 104 (2013) 176–186, https://doi.org/10.1016/j.compstruct.2013.04.005.

[23] T. I. Thinh, T. M. Tu, N. Van Long, Free vibration of a horizontal functionally graded rectangular plate submerged in fluid medium, Ocean Eng. 216 (2020) 107593, https://doi.org/10.1016/j.oceaneng.2020.107593.

[24] A. Bendahmane, S. M. Hamza-Cherif, M. N. Ouissi, Free vibration analysis of variable stiffness composite laminate (VSCL) plates coupled with fluid, Mech. Adv. Mater. Struct. 28 (2) (2021) 167–181, https://doi.org/10.1080/15376494.2018.1553257.

[25] Soedel, S.M., Soedel, W., On the free and forced vibration of a plate supporting a freely sloshing surface liquid, J. Sound. Vib. 171 (2) (1994) 159–171, https://doi.org/10.1006/jsvi.1994.1111.

[26] M. Meylan, The forced vibration of a thin plate floating on an infinite fluid, J. Sound Vib. 205 (5) (1997) 581–591, https://doi.org/10.1006/jsvi.1997.1033.

[27] S. Hosseini Hashemi, M. Karimi, H. Rokni Damavandi Taher, Vibration analysis of rectangular Mindlin plates on elastic foundations and vertically in contact with stationary fluid by the ritz method, Ocean Eng. 37 (2-3) (2010) 174–185, https://doi.org/10.1016/j.oceaneng.2009.12.001.

[28] S. Hosseini-Hashemi, M. Karimi, D. Hossein Rokni, Hydroelastic vibration and buckling of rectangular Mindlin plates on Pasternak foundations under linearly varying in-plane loads, Soil Dyn. Earthq. Eng. 30 (12) (2010) 1487–1499, https://doi.org/10.1016/j.soildyn.2010.06.019.

[29] D. Seung Cho, B. Hee Kim, J.-H. Kim, N. Vladimir, T. Muk Choi, Frequency response of rectangular plate structures in contact with fluid subjected to harmonic point excitation force, Thin-Walled Struct. 95 (2015) 276–286, https://doi.org/10.1016/j.tws.2015.07.013.

[30] S. D. Akbarov, M. I. Ismailov, S. A. Aliyev, The influence of the initial strains of the highly elastic plate on the forced vibration of the hydro-elastic system consisting of this plate, compressible viscous fluid, and rigid wall, Coupled syst. mech. 6 (4) (2017) 439–464, https://doi.org/10.12989/CSM.2017.6.4.439.

[31] S. D. Akbarov, P. G. Panakhli, On the particularities of the forced vibration of the hydro-elastic system consisting of a moving elastic plate, compressible viscous fluid and rigid wall, Coupled syst. mech. 6 (3) (2017) 287–316, https://doi.org/10.12989/CSM.2017.6.3.287.

[32] S. D. Akbarov, T. V. Huseynova, Forced vibration of the hydro-elastic system consisting of the orthotropic plate, compressible viscous fluid and rigid wall, Coupled syst. mech. 8 (3) (2019) 199–218, https://doi.org/10.12989/CSM.2019.8.3.199.

[33] Akbarov, Surkay D., Huseynova, Tarana V., On the flow of the compressible viscous fluid located between the orthotropic plate and rigid wall caused by the moving load acting on the plate, in: The 7th International Conference on Control and Optimization with Industrial Applications, Vol. 1, 2020, pp. 53–58.

[34] T. Koçal, The dynamical behavior of the moving viscoelastic plate in contact with viscous fluid with finite depth under action of time-harmonic forces, Ocean Eng. 215 (2020) 107840, https://doi.org/10.1016/j.oceaneng.2020.107840.

[35] B. E. Sandman, Fluid-loaded vibration of an elastic plate carrying a concentrated mass, J. Acoust. Soc. Am. 61 (6) (1977) 1503–1510, https://doi.org/10.1121/1.381451.

[36] A. Berry, A new formulation for the vibrations and sound radiation of fluid-loaded plates with elastic boundary conditions, J. Acoust. Soc. Am. 96 (1994) 889–901.

[37] H. Nelisse, O. Beslin, J. Nicolas, A generalized approach for the acoustic radiation from a baffled or unbaffled plate with arbitrary boundary conditions, immersed in a light or heavy fluid, J. Sound Vib. 211 (2) (1998) 207–225, https://doi.org/10.1006/jsvi.1997.1359.

[38] J. Arenas, M. Crocker, Sound radiation efficiency of a baffled rectangular plate excited by harmonic point forces using its surface resistance matrix, Int. J. Acoust. Vib. 7 (4), https://doi.org/10.20855/ijav.2002.7.4120 (2002).

[39] J.-M. Génevaux, Effect of a free-surface fluid layer on vibroacoustic response of a plate, in: 8th International Conference on Recent Advances in Structural Dynamics, 2003.

[40] Y. Sun, J. Pan, T. Yang, Effect of a fluid layer on the sound radiation of a plate and its active control, J. Sound Vib. 357 (2015) 269–284, https://doi.org/10.1016/j.jsv.2015.07.016.

[41] L. M. Brekhovskikh, Waves in layered media, Academic Press, 1960, https://doi.org/10.1063/1.3058151.

[42] P. Salaün, Effect of a free surface on the far-field pressure radiated by a point-excited cylindrical shell, J. Acoust. Soc. Am. 90 (4) (1991) 2173–2181, https://doi.org/10.1121/1.402373.

[43] T. Y. Li, Y. Y. Miao, W. B. Ye, X. Zhu, X. M. Zhu, Far-field sound radiation of a submerged cylindrical shell at finite depth from the free surface, J. Acoust. Soc. Am. 136 (3) (2014) 1054–1064, https://doi.org/10.1121/1.4890638.

[44] W. Guo, T. Li, X. Zhu, Far-field acoustic radiation and vibration of a submerged finite cylindrical shell below the free surface based on energy functional variation principle and stationary phase method, Noise Control Eng. J. 65 (6) (2017) 565–576, https://doi.org/10.3397/1/376570.

[45] P. Wang, T. Li, X. Zhu, Free flexural vibration of a cylindrical shell horizontally immersed in shallow water using the wave propagation approach, Ocean Eng. 142 (2017) 280–291, https://doi.org/10.1016/j.oceaneng.2017.07.006.

[46] V. V. Vasiliev, E. V. Morozov, Advanced Mechanics of Composite Materials and Structures (Fourth Edition), Elsevier, 2018, https://doi.org/10.1016/B978-0-08-102209-2.00018-9.

[47] J. Su, R. Vasudevan, On the radiation efficiency of infinite plates subject to a point load in water, J. Sound Vib. 208 (3) (1997) 441–455, https://doi.org/10.1006/jsvi.1997.1184.

[48] E. Lalor, Inverse wave propagator, J. Math. Phys. 9 (12) (1968) 2001–2006, https://doi.org/10.1063/1.1664535.

[49] E. G. Williams, Fourier acoustics: sound radiation and nearfield acoustical holography, Academic Press, 1999, https://doi.org/10.1016/B978-0-12-753960-7.X5000-1.

[50] H. Nelisse, O. Beslin, J. Nicolas, Fluid–structure coupling for an unbaffled elastic panel immersed in a diffuse field, J. Sound Vib. 198 (4) (1996) 485–506, https://doi.org/10.1006/jsvi.1996.0583.

[51] M. Karimi, L. Maxit, P. Croaker, O. Robin, A. Skvortsov, S. Marburg, N. Atalla, N. Kessissoglou, Analytical and numerical prediction of acoustic radiation from a panel under turbulent boundary layer excitation, J. Sound Vib. 479 (2020) 115372, https://doi.org/10.1016/j.jsv.2020.115372.

[52] E. Askari, F. Daneshmand, Free vibration of an elastic bottom plate of a partially fluid-filled cylindrical container with an internal body, Eur. J. Mech. - A/Solids 29 (1) (2010) 68–80, https://doi.org/10.1016/j.euromechsol.2009.05.005.

[53] V. H. Vu, M. Thomas, A. A. Lakis, L. Marcouiller, Effect of added mass on submerged vibrated plates, in: 25th Seminar on machinery vibration, Canadian Machinery Vibration Association, 2007.